\$ \$ \$ ELSEVIER

Contents lists available at ScienceDirect

Physica D

journal homepage: www.elsevier.com/locate/physd



Traveling waves in a spatially-distributed Wilson–Cowan model of cortex: From fronts to pulses



Jeremy D. Harris a,*, Bard Ermentrout b

- ^a Department of Biology, Emory University, Atlanta, GA, 30322, United States
- ^b Department of Mathematics, University of Pittsburgh, Pittsburgh, PA, 15260, United States

HIGHLIGHTS

- Traveling waves in a Wilson–Cowan type neural field model.
- Front-like waves that join the down state to different up states.
- Traveling breathers.
- Bistability between traveling front and pulse solutions.

ARTICLE INFO

Article history: Received 25 April 2017 Received in revised form 12 December 2017 Accepted 18 December 2017 Available online 2 January 2018 Communicated by B. Sandstede

Keywords: Neural fields Spatially-distributed networks Traveling waves

ABSTRACT

Wave propagation in excitable media has been studied in various biological, chemical, and physical systems. Waves are among the most common evoked and spontaneous organized activity seen in cortical networks. In this paper, we study traveling fronts and pulses in a spatially-extended version of the Wilson-Cowan equations, a neural firing rate model of sensory cortex having two population types: Excitatory and inhibitory. We are primarily interested in the case when the local or space-clamped dynamics has three fixed points: (1) a stable down state; (2) a saddle point with stable manifold that acts as a threshold for firing; (3) an up state having stability that depends on the time scale of the inhibition. In the case when the up state is stable, we look for wave fronts, which transition the media from a down to up state, and when the up state is unstable, we are interested in pulses, a transient increase in firing that returns to the down state. We explore the behavior of these waves as the time and space scales of the inhibitory population vary. Some interesting findings include bistability between a traveling front and pulse, fronts that join the down state to an oscillation or spatiotemporal pattern, and pulses which go through an oscillatory instability.

© 2017 Elsevier B.V. All rights reserved.

1. Introduction

Cortical waves have been observed in a variety of neural circuit experiments. Examples from slice preparation include hippocampal slices in guinea pigs [1], and rodent neocortex [2]. In addition, experimentalists have observed traveling waves *in vivo*, such as in the study of neural responses to whisker deflection in barrel cortex of anesthetized rats [3,4] and more recently, in propagation reliability in primary visual cortex of awake macaques using multichannel electrodes [5]. The authors in [6] suggest that the shape and velocity of cortical waves in neocortex may be important to understanding underlying structures of the network. Their role in sensory and motor processing ranges from inducing variability [7] to controlling motor patterns [8–13] to setting diverse phases

in sensory oscillations [14,15]. In addition, several researchers suggest that understanding the initiation and termination of so-called epileptiform events that lead to seizure activity may prove paramount for developing therapeutic techniques for seizure patients [16,17].

There is a long-standing history of studying traveling waves not only in general nonlinear systems but also in neural field models. Moreover, there has been an effort to develop theoretical models along with experimental results to qualitatively describe wave propagation and make further predictions. For instance, the authors in [18] studied the effects of GABA_A-mediated inhibitory post-synaptic potentials on the initiation, propagation, and termination of synchronous activity in slices of rat neocortex. Rather than capturing all of the synaptic dynamics as in the Hodgkin-Huxley model [19], theorists often consider a reduced model such as the FitzHugh–Nagumo equation [20,21], which does not take into account voltage-gating variables. Moreover, since many areas

^{*} Corresponding author. E-mail address: jeremy.david.harris@emory.edu (J.D. Harris).

of sensory cortex have a spatial-structure [22], neural field equations with one-dimensional continuous space can be used to model cortical waves [23]. Amari considered a scalar firing rate model given by a partial integro-differential equation. By assuming a Heaviside step function for the transfer function, he was able to analytically construct localized patterns of activity and assess their stability to determine wave propagation [24]. Since then, many others have studied traveling waves in spatially-distributed neuronal networks, including, but not limited to [25–27]. Pinto and Ermentrout studied a single population with linear adaptation using singular perturbation and were able to construct waves by separating the time scale of fast inhibition from slow inhibitory feedback [28].

In the absence of input, the cortex shows many complex spontaneous patterns. Among those which have garnered interest by physiologists are "up" and "down" states. During up states, intracellular recordings of neurons show that they are depolarized, which is due to ongoing synchronous synaptic activity. In [29], multi-electrode recordings reveal that there is a transition from down to up states in the form of a propagating wave; in other words, a wave front. In contrast, there is no such spatially organized transition from up to down states. Hence, we cannot simply propose that the fronts are traveling fronts in a scalar bistable medium [30]. Moreover, since inhibition plays a crucial role in the existence of up and down states [31], the model should involve an interplay between the excitatory and inhibitory populations.

In this paper, we describe a firing rate model for the dynamics of the space-clamped excitatory-inhibitory cortical circuit that, depending on the timescale of the inhibition is either bistable or monostable. We base this circuit on the experimental results of [31] and [32]. We embed the dynamics in a spatially-extended system of integro-differential equations in one- and two-spatial dimensions and then analyze the resulting dynamics. In the onedimensional spatial case, by our choice of spatial weighting functions, we are able to reduce the existence of traveling fronts and pulses to solving a low-dimensional dynamical system. We find that, as the inhibitory time scale increases, there are fronts (heteroclinic orbits) that join the down state to an up state characterized by a spatially-homogeneous fixed point, a bulk oscillation, or a period-doubled, spatiotemporal pattern. For slower inhibition, we show that there are pulses (homoclinic orbits) which bifurcate into periodically modulated waves as the spread of inhibition increases. We combine direct simulation of the spatially discretized systems with numerical continuation of solutions to the corresponding boundary value problem to understand the transitions and stability of the pulse and fronts. Lastly, we show simulations in two spatial dimensions and close with a discussion of our findings throughout the paper.

2. Methods

2.1. The Wilson–Cowan equations: A spatially distributed network

Large networks of synaptically connected neurons are often modeled by so-called firing rate or neural field equations [23], typically with two types of populations: Excitatory (u) and inhibitory (v). The Wilson–Cowan model is one such dynamical system that represents population activity of interconnected excitatory and inhibitory populations. We extend this model of cortex to include spatially-dependent connections with the assumption that the spatial kernels are dependent on the pre-synaptic population, but not on the post-synaptic population receiving the input:

$$\tau_e \frac{\partial u}{\partial t}(x,t) = -u(x,t) + F(a_{ee}K_e(x) \star u(x,t) - a_{ei}K_i(x)$$

$$\star v(x,t) - \theta_e)$$
(1)

$$\tau_i \frac{\partial v}{\partial t}(x, t) = -v(x, t) + F(a_{ie}K_e(x) \star u(x, t) - a_{ii}K_i(x)$$

$$\star v(x, t) - \theta_i)$$

where u, v are the firing rates of the excitatory and inhibitory populations, respectively, F(I) is a nonlinear function representing the firing rate as a function of the spatially distributed inputs: $K_j(x)$, $j \in \{e, i\}$ are spatial interaction functions (typically Gaussian or exponentially decaying with distance) which are convolved with the activities. Here, $k(x) \star m(x) := \int_D k(x-y) m(y) \ dy$, where D is the spatial domain of the network. The parameters $\tau_j, j \in \{e, i\}$ represent the time scales of the excitatory and inhibitory activities; the parameters a_{jk} are the coupling strengths from population k to population j and θ_j are thresholds. Throughout this paper, we let $F(I) = 1/(1 + \exp(-\beta I))$ and $\beta = 50$, $a_{ee} = a_{ie} = 1$, $a_{ei} = 1.5$, $a_{ii} = 0.25$, $\theta_e = 0.125$, $\theta_i = 0.4$. Since we can rescale time, without loss of generality, we set $\tau_e = 1$ so that $\tau = \tau_i$ is the relative time constant of inhibition to excitation. The parameters $\sigma_j, j \in \{e, i\}$ are the spatial length scales of the excitatory and inhibitory connections:

$$K_e(x) = \frac{1}{2\sigma_e} \exp\left(-\frac{|x|}{\sigma_e}\right)$$
 and $K_i(x) = \frac{1}{2\sigma_i} \exp\left(-\frac{|x|}{\sigma_i}\right)$,

normalized so that $\int_{\mathbb{R}} K_{\varrho}(x) dx = \int_{\mathbb{R}} K_{i}(x) dx = 1$. Though Gaussian kernels yield similar results, we choose exponential kernels to facilitate with mathematical analysis. (See Fig. 1).

Throughout this manuscript, we focus on the time and space constants of the inhibitory feedback, both of which have been shown to be important in the dynamics of cortex. Then when we consider the full network model with both excitatory and inhibitory spatially-distributed connections, we will fix the time and space constants of excitation to be one, i.e. $\tau_e = \sigma_e = 1$, so that the temporal and spatial scales of the network, denoted $\tau = \tau_i/\tau$ and $\sigma = \sigma_i/\sigma_e$, are those of inhibition *relative* to excitation.

We want to study two types of traveling waves: The first is a traveling front of activity that transitions the media from a down state (low firing rate) to an up state (high firing rate). This type of network-level propagation and activation has been studied for its relation to epileptiform behavior during seizure activity; the second waveform is the traveling pulse which has been observed experimentally in several areas of animal cortex such as in the whisker barrel circuit of rat cortex. To better understand the wave fronts that transition from the down state to the up state, we must first describe the behavior of these two states, both in the space-clamped model ("zero-dimensional" with no space) and in the spatially-extended system.

2.2. The E-I system without spatial coupling

As long as the spatial kernels are normalized, the space-clamped system (when all solutions are independent of x) reduce to the classical Wilson–Cowan equations:

$$u' = -u + F(a_{ee} u - a_{ei} v - \theta_e)$$

$$\tau v' = -v + F(a_{ie} u - a_{ii} v - \theta_i),$$
(2)

where $'=\frac{d}{dt}$ and $\tau=\tau_i/\tau$ is the time constant of inhibition relative to excitation. For the chosen set of parameters, there are three equilibria: (1) The down state (\bar{u}_1,\bar{v}_1) ; (2) the saddle point (\bar{u}_2,\bar{v}_2) ; and (3) the up state equilibrium (\bar{u}_3,\bar{v}_3) , which, in the case that it is stable, has been referred to as the Inhibitory Stabilized Network (ISN) state [32,33]. Fig. 2B shows the configuration of the nullclines with the given parameter set. The three fixed points satisfy

$$0 = -u + F(a_{ee} u - a_{ei} v - \theta_e)$$

$$0 = -v + F(a_{ie} u - a_{ii} v - \theta_i).$$
(3)

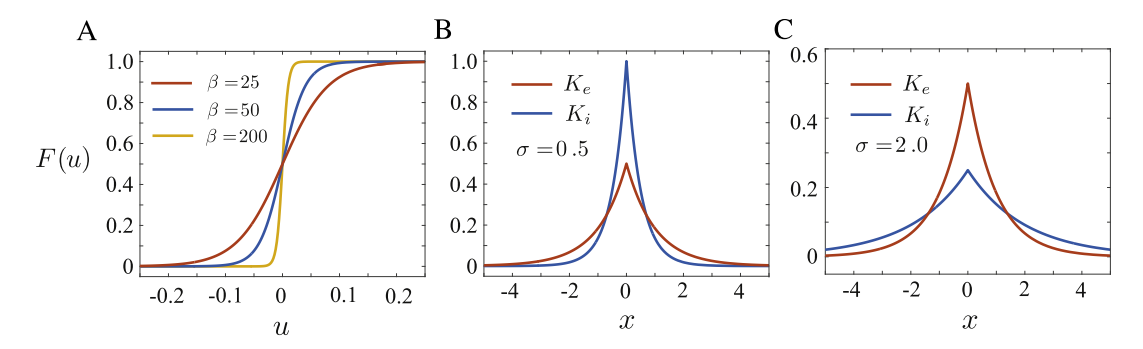


Fig. 1. The firing rate function and spatial kernels. (A) The sigmoidal firing rate function with increasing gain parameter: $\beta = [25, 50, 200]$. (B) The excitatory (K_e) and inhibitory (K_i) kernels without lateral inhibition: $\sigma < 1$. (C) Excitatory and inhibitory kernels in the case of lateral inhibition $\sigma > 1$.

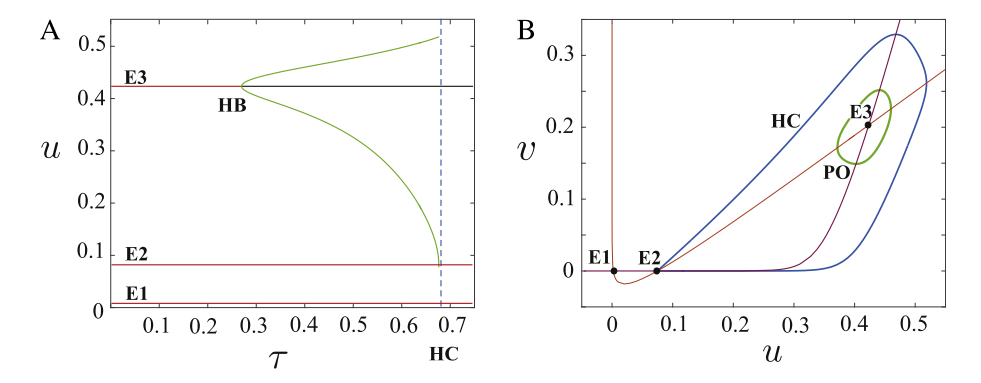


Fig. 2. The space-clamped dynamics. (A) The bifurcation diagram with u-values plotted against the relative time constant of inhibition $\tau > 0$. The top horizontal red curve is the stable up state (E3) that goes through a supercritical Hopf Bifurcation (HB) at $\tau_{HB} = 0.2697$. The green curve corresponds to stable limit cycles which terminate at the Homoclinic Bifurcation (HC), shown with a vertical dashed line at $\tau_{HC} = 0.6764$. (B) The u-v phase plane: The u-nullcline (orange) and v-nullcline (violet), the three equilibria E1, E2, E3, a periodic orbit (PO) for $\tau = 0.4$ and a homoclinic connecting the unstable and stable manifolds of saddle point (E2). (For interpretation of the references to color in this figure legend, the reader is referred to the web version of this article.)

As we will see shortly, the lower left equilibrium, E1, is the down state which is unconditionally asymptotically stable; the middle state, E2, is always a saddle point, and the right-most fixed point, E3, is the stable up state if τ is sufficiently small. We note that the up state is on the middle branch of the cubic nullcline rather than on the right branch. In chapter 11 of [34], the authors argue that this nullcline configuration (with a fixed point on the middle branch) is the only one that can explain the properties of up and down states to stimuli [31]. Moreover, this configuration has been used to explain the paradoxical effects of a sustained drive to the inhibitory population which decreases the firing rate of the excitatory and inhibitory populations [32,33].

We can understand the stability of the equilibria from the linearization about each of them which is given by the matrix, A_0 :

$$A_0 = \begin{pmatrix} -1 + b_{ee} & -b_{ei} \\ b_{ie}/\tau & -(1 + b_{ii})/\tau \end{pmatrix}.$$

Here $b_{jk}=a_{jk}F'(a_{je}\bar{u}-a_{ji}\bar{v}-\theta_j)$, for $j,k\in\{e,i\}$. Since $F'(\cdot)>0$, each of the $b_{jk}\geq 0$. Since the down state lies on the negatively sloped branch of the excitatory nullcline, then $-1+b_{ee}<0$, and so the trace (determinant) of A_0 is negative (positive) and the down state is stable for all values of τ . The middle equilibrium, E2, lies on a point where the slope of the excitatory nullcline exceeds that of the inhibitory so it is always a saddle point which has a stable manifold that acts as a separatrix of the phase plane. That is, for small perturbations of the rest state, the activity tends back to rest, but for sufficiently large perturbations past the separatrix, the trajectory may go away from the down state. Depending on the stability of the up state, E3, the trajectory may tend to E3, to a limit cycle surrounding E3, or make an excursion around E3 and fall back down to rest. We note that at the up state, the slope

of the inhibitory nullcline is greater than that of the excitatory nullcline so it is always a source or a sink (the determinant is always positive) depending on the trace of A_0 . For the parameters of interest, we can show that for small $\tau>0$, the trace and discriminant are both negative, so we have complex conjugate eigenvalues with negative real part. As we increase $\tau>0$, the trace increases through zero while the discriminant remains negative. Hence, the fixed point goes through a Hopf bifurcation at $\tau=\tau_{HB}$, where

$$\tau_{HB} = (1 + b_{ii})/(b_{ee} - 1) = (1 + a_{ii} \beta \bar{v}(1 - \bar{v}))/(\beta \bar{u}(1 - \bar{u}) - 1),$$

which for our parameters is approximately $\tau_{HB} = 0.2697$.

In Fig. 2A, we show the change in stability: For small $\tau > 0$, E3 is a stable fixed point (red horizontal line), and as τ increases, the fixed point goes through a supercritical Hopf Bifurcation from which limit cycles emerge (green curves in Fig. 2A). The limit cycles grow with increasing τ and terminate at a homoclinic bifurcation (vertical, dashed blue line in Fig. 2A) which connects the unstable manifold (as $t \to -\infty$) to the stable manifold (as $t \to \infty$) of the saddle point (blue curve in Fig. 2B). This bifurcation will be important not only for finding the homoclinic orbit that corresponds to a traveling pulse, but also for understanding how the network transitions from supporting a front to a pulse waveform as the time constant of inhibition increases. To summarize the equilibria and stability of the space-clamped system, E1 is always a stable fixed point, E2 is always a saddle point, and E3 is a spiral node with stability depending on the time constant of inhibition: For small τ , the up state is a stable fixed point; for τ slightly greater than τ_{HB} , the up state consists of a stable limit cycle; for $\tau > \tau_{HC}$, there are no stable up states.

2.3. Pattern formation in the up state

Before we study the traveling waves, which involves the spatially-distributed network, we want to determine the behavior of the up states within the spatially-distributed network. Since the traveling fronts join the down to up states, then at the very least, we want there to be some type of stable up state dynamics. In the previous section, we showed that the equilibrium up state of the homogeneous (space-clamped) system was unstable once the inhibition time constant, τ , exceeded τ_{HB} (the Hopf bifurcation), which gives rise to periodic orbits. The oscillatory up state persisted until it was lost at a homoclinic bifurcation. In this section, we examine the stability of these spatially homogeneous states in the spatially-extended network. We first note that since $b_{ee} < 1$ in the down state, a pattern forming instability is not possible in this lower state, so we restrict our attention to the up state.

2.3.1. Stationary patterns

We first want to determine whether a stationary pattern may arise from perturbations of the up state when $0 < \tau < \tau_{HB}$. For the perturbation analysis, we will denote the up state equilibrium by $(\bar{u}, \ \bar{v}) = (\bar{u}_3, \ \bar{v}_3)$ and consider a perturbed solution of the form

$$U(x, t) = \bar{u} + \varepsilon u(t) e^{i\omega x}$$
, $V(x) = \bar{v} + \varepsilon v(t) e^{i\omega x}$,

so that the convolutions become

$$K_{e}(x) \star U(x,t) = \bar{u} + \varepsilon \, \hat{K}_{e}(\omega) \, u(t) \, e^{i\omega x}$$

$$K_{i}(x) \star V(x,t) = \bar{v} + \varepsilon \, \hat{K}_{i}(\omega) \, v(t) \, e^{i\omega x} \,,$$

$$(4)$$

where $\hat{K}_{j}(\omega)$ are the Fourier transforms of $K_{j}(x)$. We plug (4) into (1) and take a Taylor expansion. Using the constant steady-state conditions in (3), we collect order ε terms to obtain a family of linear two-dimensional ODEs parametrized by wavenumber, ω :

$$u_t = -u + b_{ee}\hat{K}_e(\omega)u - b_{ei}\hat{K}_i(\omega)v$$

$$\tau v_t = -v + b_{ie}\hat{K}_e(\omega)u - b_{ii}\hat{K}_i(\omega)v,$$
(5)

where b_{jk} are constants $b_{jk} = a_{jk} F'(a_{j,e} \bar{u} - a_{j,i} \bar{v} - \theta_j)$. Then the linearization is a family of matrices which are parametrized by ω ,

$$A(\omega) = \begin{pmatrix} -1 + b_{ee}\hat{K}_e(\omega) & -b_{ei}\hat{K}_i(\omega) \\ \left(b_{ie}\hat{K}_e(\omega)\right)/\tau & \left(-1 - b_{ii}\hat{K}_i(\omega)\right)/\tau \end{pmatrix}.$$

By the choice of firing rate function, F satisfies the logistic equation, $F' = \beta F (1 - F)$. Now, since (\bar{u}, \bar{v}) satisfy (3), we obtain $b_{je} = a_{je} \beta \bar{u} (1 - \bar{u})$ and $b_{ji} = a_{ji} \beta \bar{v} (1 - \bar{v})$. Then the trace of $A(\omega)$ is $\mathrm{Tr}(\omega) = b_{ee} \hat{K}_e(\omega) - 1 - \left(1 + b_{ii} \hat{K}_i(\omega)\right) / \tau$. For the case that we study here, the trace is negative for small $\tau > 0$. Then the only way for an instability to occur is for the determinant to be positive at $\omega = 0$ and become negative for some positive value of ω . We consider $D(\omega) = \left(1 - b_{ee} \hat{K}_e(\omega)\right) \left(1 + b_{ii} \hat{K}_i(\omega)\right) + b_{ei} b_{ie} \hat{K}_i(\omega) \hat{K}_e(\omega)$, which is τ multiplied by the determinant of $A(\omega)$ and see that

$$\begin{split} D(0) &= (1-b_{ee}) \, (1+b_{ii}) + b_{ei} \, b_{ie} \\ &= (1-\beta \bar{u}(1-\bar{u})) \, (1+a_{ii} \, \beta \bar{v} \, (1-\bar{v})) \\ &+ a_{ei} \, \beta^2 \, \bar{u} \, (1-\bar{u}) \, \bar{v} \, (1-\bar{v}) \\ &= 1+\beta \, \left(a_{ii} \, \bar{v} \, (1-\bar{v}) - \bar{u} \, (1-\bar{u}) \right) \\ &+ \beta^2 \, (a_{ei} - a_{ij}) \, \bar{u} \, (1-\bar{u}) \, \bar{v} \, (1-\bar{v}) \, . \end{split}$$

As noted in the previous section, the determinant of the space-clamped system is always positive, so D(0) > 0. Then, considering $D(\omega)$ for $\omega > 0$, we have

$$D(\omega) = 1 + \beta (a_{ii} K_i(\omega) \bar{v} (1 - \bar{v}) - K_e(\omega) \bar{u} (1 - \bar{u}))$$

+ $\beta^2 (a_{ei} - a_{ii}) \bar{u} (1 - \bar{u}) \bar{v} (1 - \bar{v}) K_i(\omega) K_e(\omega)$.

In Fig. 3A, we graph the function $D(\omega)$ and see that $\sigma=\sigma_i/\sigma_e$ must be greater than one in order for the spatially-homogeneous constant solution to go unstable. In addition, we show the Turing stripes that can arise as a stationary pattern in Fig. 3B.

2.3.2. Spatiotemporal patterns

To continue with our analysis of the up state, we consider the spatially-extended network when there is a periodic up state, which occurs for the range of inhibitory time constants, $\tau_{HB} < \tau < \tau_{HC}$. This periodic up state is a bulk oscillation of the spatially-extended network and corresponds to a periodic orbit of the space-clamped system in Eq. (2). The authors of [35] study spatiotemporal pattern formation in Eq. (1) by considering a similar perturbation as in the previous section, but instead, from the spatially-homogeneous, periodic orbit, $(\bar{u}(t), \bar{v}(t))$. The dynamics of the perturbation are given by the family of time dependent matrices, parametrized by wavenumber, ω :

$$A(t;\omega) = \begin{pmatrix} -1 + b_{ee}(t)\hat{K}_e(\omega) & -b_{ei}(t)\hat{K}_i(\omega) \\ \left(b_{ie}(t)\hat{K}_e(\omega)\right)/\tau & \left(-1 - b_{ii}(t)\hat{K}_i(\omega)\right)/\tau \end{pmatrix},$$

where $b_{ek}(t) = a_{ek} F'(a_{ee} \bar{u}(t) - a_{ei} \bar{v}(t) - \theta_e)$ and $b_{ik}(t) = a_{ik} F'(a_{ie} \bar{u}(t) - a_{ii} \bar{v}(t) - \theta_i)$ for $k \in \{e, i\}$. For a fixed ω , we solve for the T-periodic orbit of the linear system $X' = A(t; \omega)X$ with initial conditions, X = I, where I is the 2 by 2 identity matrix. This forms the principal matrix of solutions, $X(t; \omega)$, which we evaluate after one period to obtain the Monodromy matrix $M(\omega) := X(T; \omega)$. The authors of [35] find that the periodic orbit loses stability through a period-doubling bifurcation, whereby a real eigenvalue of $M(\omega)$ decreases below -1. Hence the periodic orbit is unstable to perturbations of wave numbers that satisfy

$$Q(\omega) := 1 + Tr(\omega) + D(\omega) < 0,$$

where $\text{Tr}(\omega)$ and $\text{D}(\omega)$ denote the trace and determinant of the Monodromy matrix.

For $0 < \sigma < 1$, the graph of $Q(\omega)$ has a quadratic shape that dips below zero for an interval of wave numbers. As we vary a parameter, say σ , the zeros come together at a double root. This gives a minimal value of σ for which instabilities to the bulk oscillation can occur. In Fig. 4A, we show the lower pattern forming boundary (PF) in (σ, τ) parameter space: Above PF, the spatiallyextended network has an unstable periodic orbit (UO); below PF, there is either a stable periodic orbit (above the Hopf, HB) or a stable fixed point (below HB). A spatiotemporal pattern is shown in Fig. 4B when $(\sigma, \tau) = (0.8, 0.5)$. These are the same parameter values as in Fig. 6C(iii), which shows a similar spatiotemporal pattern left in the wake of the front. We see that in the absence of inhibitory connections ($\sigma=0$) there is an interval of au-values for which the periodic orbit goes unstable. We will see that there can be fronts that join the down state to this complex spatio-temporal up state.

Summarizing, we have shown that the down state consists only of a stable equilibrium point and that the up state can be one of four different types: a stable spatially uniform equilibrium; a stable spatially uniform oscillation; a stable spatially periodic pattern; or a complex spatio-temporal pattern. By varying the time constant or the spatial spread of inhibition, we are able to find these different regimes as shown in Fig. 4A. (Note that the regime of time-independent spatial patterns is not shown in this diagram as it occurs for σ outside the range shown here.)

2.4. A system of partial differential equations: Localized inhibition

To study traveling waves, we first focus on Eq. (1) when there is only localized inhibition, i.e. $\sigma = \sigma_i = 0$. In this case, the transfer function of the inhibitory dynamics only has spatial dependence through the excitatory interaction kernels. By judicious

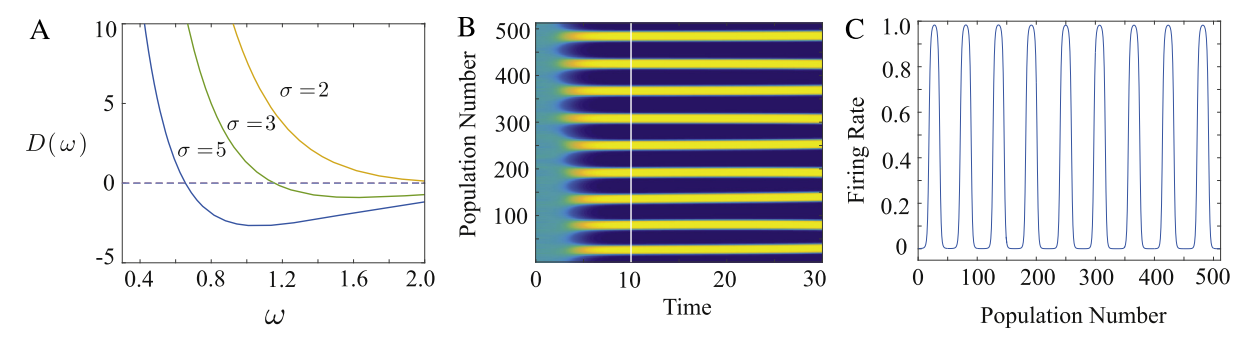


Fig. 3. Stationary patterns. (A) The graph of $D(\omega)$ for three values: $\sigma = [2, 3, 5]$ to show the Turing-instability as the spatial spread of inhibition increases in the system. (B) Turing stripes of the excitatory population array for N = 512, when $\sigma = 3$ and $\tau = 0.1$. (C) A cross-section (vertical, white line) of the time-invariant stripes from the excitatory array in panel (B) at time t = 10.

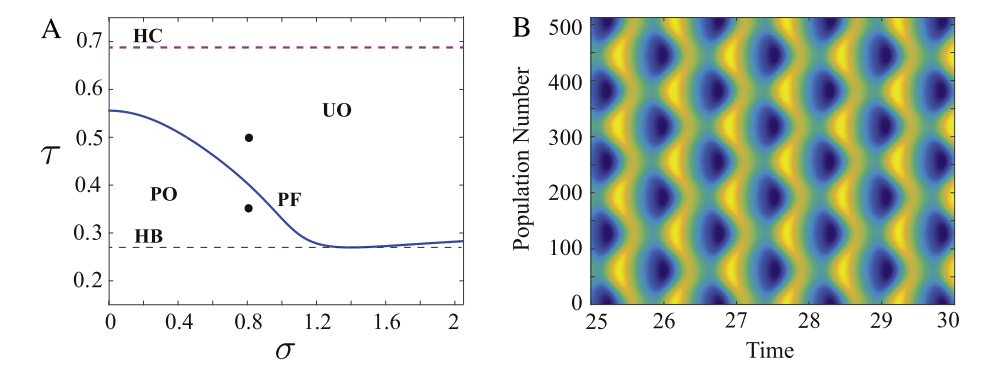


Fig. 4. Spatiotemporal Pattern Formation. (A) Stability diagram for the homogeneous periodic orbit (PO) as the σ and τ vary. The (violet) horizontal dashed line is the homoclinic (HC) for $\theta_e = 0.125$. The lower boundary (PF) has a lower bound at the Hopf Bifurcation (HB). Below the HB line, the up state is a stable equilibrium point. The black dots are $(\sigma, \tau) = (0.8, 0.35)$, $(\sigma, \tau) = (0.8, 0.5)$, and correspond to values in Fig. 6B, C (ii), (iii). (B) Period-doubled patterns of the excitatory population array for N = 512 when $\sigma = 0.8$ and $\tau = 0.5$. (For interpretation of the references to color in this figure legend, the reader is referred to the web version of this article.)

choice of weight kernel, namely the exponential that decays with distance, we can convert the partial integro-differential equation to an equivalent 4D system of partial differential equations using similar techniques as in [36,37]. Specifically, we let $w=w(x,t):=K_e(x)\star u(x,t)$ denote the convolved excitatory activity; taking two partial derivatives with respect to x, one can show that w satisfies the second order partial differential equation: $\frac{\partial^2 w}{\partial x^2}=(w-u)/\sigma_e^2$. Then, defining $z=z(x,t):=\frac{\partial w}{\partial x}$, we can write the partial integrodifferential equation in (1), assuming localized inhibition, as

$$\frac{\partial u}{\partial t} = -u + F(a_{ee} w - a_{ei} v - \theta_e)
\tau \frac{\partial v}{\partial t} = (-v + F(a_{ie} w - a_{ii} v - \theta_i))
\frac{\partial w}{\partial x} = z
\frac{\partial z}{\partial x} = (w - u)/\sigma_e^2.$$
(6)

This is a system of four coupled PDEs. If we include nonlocal inhibition, we can apply the same trick to get six coupled first order PDEs.

In the coming sections, we will explore the traveling wave solution of (6) and then follow the orbits of this 4D system embedded in the full 6D system. In the next section, we introduce the traveling wave frame ($\xi = x + \eta t$), and the PDEs become ODEs of the same dimension in this coordinate system. The solutions of the 6D system, are approximated through a decomposed shooting method, which decouples the 6D system into a 4D+2D set of ODEs. This technique allows us to numerically approximate the traveling wave solutions of Eq. (1) by a homotopy of solutions from the 4D to the full 6D model when $\sigma_i > 0$ using continuation methods.

2.5. The traveling wave frame

In the next sections, we study the two traveling wave solutions to Eq. (6): 1. A traveling front solution, where the mean firing rate of E and I populations transitions from a down to up state; 2. A traveling pulse solution, where the E and I populations transiently increase their firing rates, make an excursion around the up state and then decay back to the down state. In particular, we analyze how the inhibitory time constant transitions the system from traveling fronts to traveling pulses. Later, when we consider the fully coupled 6D system, another bifurcation parameter of interest is the spatial length scale of inhibition, which for $\sigma_e > 0$, can be studied in terms of the relative spatial spread of inhibition to excitation given by the ratio $\sigma = \sigma_i/\sigma_e$.

These waveforms can be analyzed within the traveling wave frame, $\xi=x+\eta\,t$, where $\eta>0$ is the unknown velocity of the wave. If we suppose solutions of the form $U(x,t)=u(\xi)$, $V(x,t)=v(\xi)$, then $\frac{\partial}{\partial x}=\frac{d}{d\xi}$, and the chain rule yields $\frac{\partial}{\partial t}=\eta\,\frac{d}{d\xi}$. In phase space, the traveling waves correspond to homoclinic (pulse) or heteroclinic (front) orbits; these are trajectories that connect a single equilibrium or two distinct equilibria, respectively, in the limit as $\xi\to\pm\infty$. Denoting $'=\frac{d}{d\xi}$, we obtain a 4-dimensional system of first-order differential equations:

$$\eta u' = (-u + F(a_{ee} w - a_{ei} v - \theta_{e}))
(\eta \tau) v' = (-v + F(a_{ie} w - a_{ii} v - \theta_{i}))
w' = z
z' = (w - u)/\sigma_{e}^{2},$$
(7)

where $\eta>0$ is the unknown wave speed. There are three fixed points of the system, just as in the space-clamped system, which we denote $(u,v,w,z)_{\mu}=(\bar{u},\bar{v},\bar{u},0)_{\mu}$, where $\mu=1$ for the down state, $\mu=2$ for the saddle point, and $\mu=3$ for the up state.

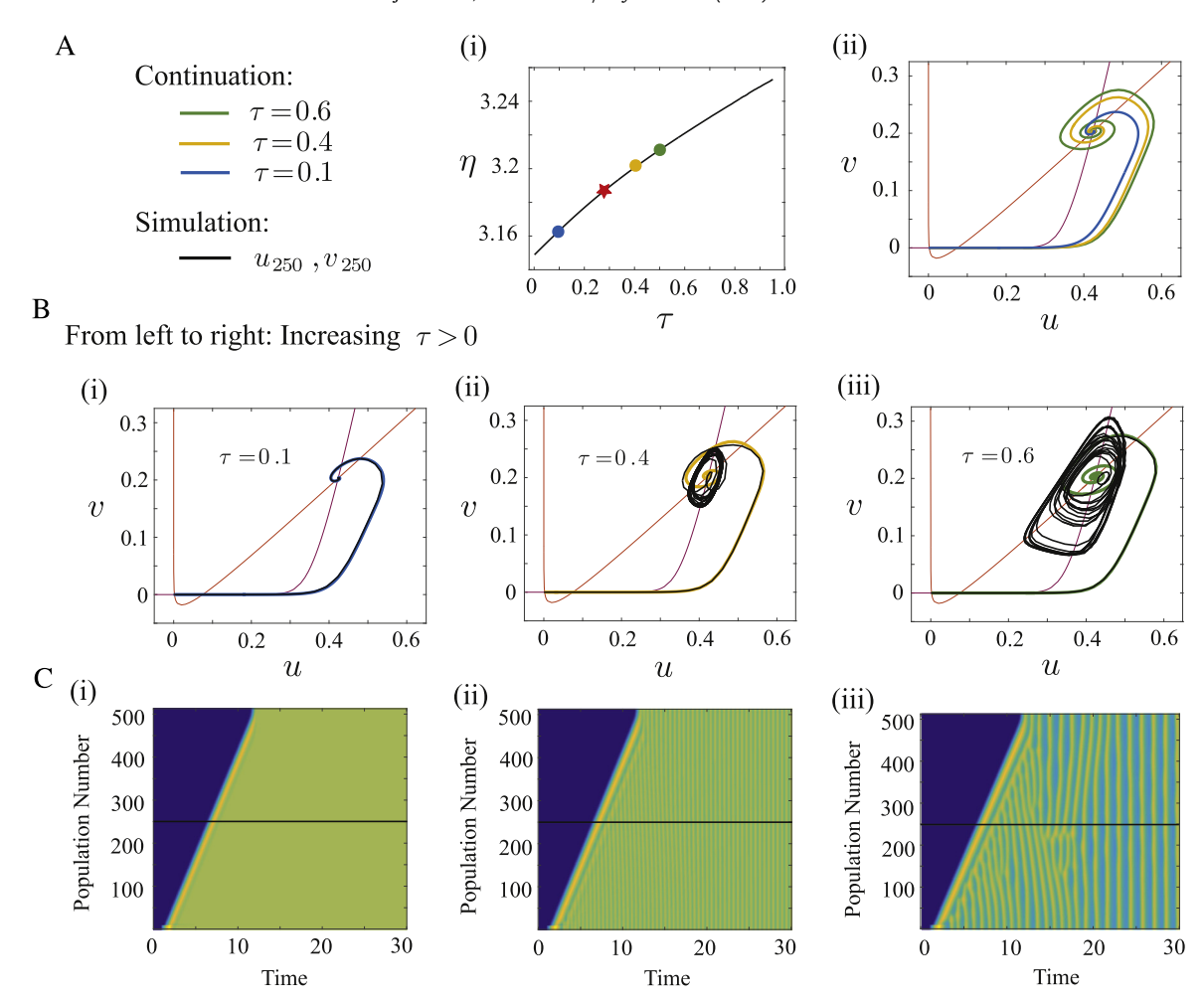


Fig. 5. Comparison of traveling front solutions of the boundary value problem and simulations of the discretized network of N=512 excitatory and inhibitory neurons with local inhibitory connections ($\sigma_i=0$). (A) In panel (i), we continue the traveling front solution with respect to (τ , η). The red star indicates an instability (computed numerically) of the front at $\tau=0.2923$. In panel (ii), we show the three different solutions for $\tau=[0.1,0.4,0.6]$. (B) The u-v phase planes: (i) $\tau=0.1$: The system tends to the constant steady-state E3; (ii) $\tau=0.4$: The firing rate increases and tends to a spatially-homogeneous limit cycle around the up state; (iii) $\tau=0.6$: The stimulated system increases in activity and moves away from the spatially homogeneous periodic orbit (bulk oscillation) toward a period-doubled oscillation (spatiotemporal pattern). (C) The three tendencies are shown in the corresponding array plots of the excitatory population firing rates. Horizontal, white lines denote the temporal dynamics projected in (B).

2.5.1. The traveling front: Localized inhibition

We first consider when $\tau < \tau_{HB}$ and determine parameters for the existence of a traveling front with wave speed $\eta > 0$. This solution corresponds to a heteroclinic orbit which connects the unstable manifold of the down state, $(u,v,w,z)_1=(\bar{u},\bar{v},\bar{u},0)_1$ to the stable manifold of the up state, $(u,v,w,z)_3=(\bar{u},\bar{v},\bar{u},0)_3$. Hence, the boundary conditions satisfy

$$\lim_{\xi \to -\infty} (u, v, w, z) (\xi) = (\bar{u}, \bar{v}, \bar{u}, 0)_{1}$$

$$\lim_{\xi \to \infty} (u, v, w, z) (\xi) = (\bar{u}, \bar{v}, \bar{u}, 0)_{3}.$$
(8)

The linearization around the down and up states is given by

$$M_{\mu} = \begin{pmatrix} -1/\eta & -b_{ei}/\eta & b_{ee}/\eta & 0 \\ 0 & (-1-b_{ii})/(\eta \tau) & b_{ie}/(\eta \tau) & 0 \\ 0 & 0 & 0 & 1 \\ -1/\sigma_e^2 & 0 & 1/\sigma_e^2 & 0 \end{pmatrix},$$

where $b_{ke} = a_{ke} \beta \bar{u} (1 - \bar{u})$ and $b_{ki} = a_{ki} \beta \bar{v} (1 - \bar{v})$, evaluated at the fixed points: $(u, v, w, z)_{\mu}$, $\mu = 1, 3$. In Appendix A, we show that M_1 has exactly one positive eigenvalue and the remaining eigenvalues have negative real parts. We also show that as long as the up state is a stable solution to the space-clamped system

in (2), then the matrix M_3 has one positive eigenvalue and the remaining three eigenvalues have negative real parts (for all $\eta>0$). Thus, there is a one-dimensional unstable manifold for the down state equilibrium which gives us an approximate starting point for our numerical shooting. We note that the dimensions of these manifolds may be preserved outside the range of parameters where the up state is stable. So, as we will see, the existence of a front joining the down state to the up state persists well beyond the range of parameters where the up state is a stable equilibrium point.

In Fig. 5, we approximate the heteroclinic with a one-dimensional shooting method in which we fix $\tau=0.1$ and then vary $\eta>0$ to obtain a trajectory (of finite period) that connects to the stable manifold of the up state. We refine this estimate using AUTO [38] by extending the period to a large number (10^4). We then continue in the desired parameter. In Fig. 5A(ii), we show the curve of heteroclinics in (τ,η) parameter space and note that as the inhibition slows down, the wave velocity increases. Intuitively, if the inhibition is slower, then the excitation has a chance to excite the down state before the inhibition gets a chance to kick in. In Fig. 5A(ii), we show several trajectories for various time constants. We note that the heteroclinic orbit has been continued up to τ nearly 1 in Fig. 5A(i), which is well past the values of τ for which the up state is a stable equilibrium in the space-clamped system

(cf Fig. 2A, where $\tau_{HB} \approx 0.27$, $\tau_{HC} \approx 0.67$). We find from our numerical stability analysis (described in Appendix E) that for σ_i = 0 the front loses stability at around $\tau = 0.2923$ (indicated by a star in Fig. 5A(i)) as a pair of complex eigenvalues passes through the imaginary axis. In Fig. 5B, we superimpose the simulations of the discretized network with N = 512 onto our numerical approximation of the heteroclinic in the u-v phase plane. To initialize the wave in the discretized system, we excite a small portion of the medium and then check to see that a wave propagates. For $\tau < \tau_{HB}$, we see that the excitation propagates as a front and that the shooting and simulations of the full network match very well (Fig. 5B(i)). However, when $\tau > \tau_{HB}$, the up state equilibrium is no longer a stable fixed point for the space-clamped system, and this is demonstrated in panels (ii) and (iii) of Fig. 5B, C. In panel (ii), $\tau =$ $0.4 > \tau_{HB}$ and we observe that instead of joining the down state to a fixed point, as seen in the shooting method, the full spatially discretized system shows a wave that connects the down state to a spatially homogeneous oscillation. For even larger τ , the full system appears to join the down state to a complex spatiotemporal pattern. Such patterns arise through a period-doubling bifurcation of a spatially homogeneous oscillation (see Fig. 4). In all three cases shown in Fig. 5B, the portion of the trajectory from the down state out to the maximum value of u is the same for both the shooting and the simulation of the full spatial model. For this reason, the velocity of the front is predicted by the shooting even though the asymptotic up state is not the equilibrium point required by the shooting. Thus, while our shooting method does not technically apply for values of $\tau > \tau_{HB}$, it provides an almost exact predictor for the velocity of the transition, since the solutions mostly agree with simulations during the up stroke of propagation. Fig. 5A(ii) shows the front velocity only up to $\tau \approx 0.95$, beyond which we were unable to continue the solution. If we choose τ close to 1, then instead of fronts, we see pulses in the spatially discretized system. These will be analyzed in Section 2.5.3.

2.5.2. The traveling front: Nonlocal inhibition

By introducing nonlocal coupling of the inhibitory population, the system in Eq. (6) increases to a 6D system of first order differential equations given by

$$\eta u' = (-u + F(a_{ee} w - a_{ei} q - \theta_e))
(\eta \tau) v' = (-v + F(a_{ie} w - a_{ii} q - \theta_i))
w' = z
z' = (w - u)
q' = r
r' = (q - v)/\sigma^2,$$
(9)

where q, r are the additional variables to represent the convolution $(K_i \star v)(x)$ as a second order system, and $\sigma = \sigma_i/\sigma_e$ is the relative length scale of inhibition to excitation. Similar to the 4D system, we write the boundary conditions for the traveling front (with wave speed $\eta > 0$). In the phase plane, this corresponds to a heteroclinic orbit with the following boundary conditions:

$$\lim_{\xi \to -\infty} (u, v, w, z, q, r) (\xi) = (\bar{u}, \bar{v}, \bar{u}, 0, \bar{v}, 0)_{1}$$

$$\lim_{\xi \to \infty} (u, v, w, z, q, r) (\xi) = (\bar{u}, \bar{v}, \bar{u}, 0, \bar{v}, 0)_{3}.$$
(10)

The linearization of the full 6D system in Eq. (9) around the down and up states is given by

$$M_{\mu} = \begin{pmatrix} -1/\eta & 0 & b_{ee}/\eta & 0 & -b_{ei}/\eta & 0 \\ 0 & -1/(\eta\,\tau) & b_{ie}/(\eta\,\tau) & 0 & -b_{ii}/(\eta\,\tau) & 0 \\ 0 & 0 & 0 & 1 & 0 & 0 \\ -1 & 0 & 1 & 0 & 0 & 0 \\ 0 & 0 & 0 & 0 & 0 & 1 \\ 0 & -1/\sigma^2 & 0 & 0 & 1/\sigma^2 & 0 \end{pmatrix},$$

where $b_{ek} = a_{ek} \ \beta \ \bar{u} \ (1 - \bar{u})$ and $b_{ik} = a_{ik} \beta \ \bar{v} \ (1 - \bar{v})$. In Appendix A, we show that the down state has a two-dimensional unstable subspace and a four-dimensional stable subspace. We also show that if the up state is a stable equilibrium of the space-clamped system in (2), then the dimensions of the stable and unstable subspaces are the same as those of the down state. Since the unstable space has a dimension greater than one, the numerical shooting is more difficult to implement than in the 4-dimensional ODE. More precisely, in the case of 4-dimensions, only one parameter (e.g. η) needs to be varied to approximate the heteroclinic and homoclinic orbits , while in the present case of 6-dimensions, two parameters (e.g. η and another parameter to adjust the angle along the two-dimensional unstable subspace) must be varied.

We thus use numerical solutions of the 4D system in Eq. (7) to shoot in the higher dimensional system in which the variables q, r are decoupled from the dynamics of the 4D system (but not viceversa). From this, we can obtain a decent approximation for the solution of Eq. (9) when $0 < \sigma_i \ll 1$. We then perform a homotopy from one system to the next using numerical continuation of a parameter, say λ , from 0 to 1, where $\lambda=0$ gives the solution of Eq. (7) and $\lambda=1$ gives the solution to Eq. (9) when the inhibitory population has nonlocal, spatially-distributed connections. We provide further explanation of this procedure along with detailed equations for the homotopy in Appendix B.

Fig. 6A depicts the velocity of the traveling front solutions to Eq. (9) when both excitation and inhibition have nonlocal, spatially-distributed connections. In Fig. 6A(i), we fix $\sigma=0.8$ and vary τ against η . Then in Fig. 6A(ii), we plot the curve of fronts in (σ,η) parameter space for fixed values of $\tau=[0.1,0.35,0.5]$ and see that as σ increases, the velocity of the traveling front tends to zero. Moreover, the velocity monotonically decreases with increasing spatial spread of inhibition which suggests that the longer reach of inhibition more strongly suppresses excitation of the down state. This extends the onset of the pulse, which slows propagation of the wave. The behavior of the velocity as τ varies, shown in Fig. 6A(i), is qualitatively the same as in Fig. 5A(i); it is just slower as expected from Fig. 6A(ii).

In Fig. 6B, we let $\sigma = 0.8$ and find transitions which are similar to those found in Fig. 5B. For $\tau = 0.1$, the up state is stable and we see a transition of the system from the down state to the up state. As we increase τ to 0.35, a limit-cycle emerges around the unstable fixed point for the space-clamped system. Despite this, the curve of traveling fronts continues in (τ, η) space, so in Fig. 6B(ii) and (iii), we superimpose network simulations of the discretized spatial system onto numerical solutions and project them in the u-v phase plane. Since the spatially uniform up state is unstable, the network tends to a bulk oscillation similar to the limit-cycle depicted in Fig. 2B. When $\tau = 0.5$, the spatially homogeneous oscillation is unstable and the system tends to a spatiotemporal pattern, which can be seen in the excitatory array plot in Fig. 6C(iii) (cf. Fig. 4B). Thus, we see that the effect of spatial connectivity of the inhibition has little qualitative effect on the form of the waves, both in the shooting and the full simulation. However, we note that the velocity is very strongly dependent on σ with the maximum effect occurring around $\sigma = 1$. That is, the velocity of the wave is very sensitive to the lateral connectivity of the inhibitory neurons when that connectivity has roughly the same spatial spread as the excitatory population. For nonlocal inhibition, the transition from the down state to a spatiotemporal patterned up state at higher values of τ is much more apparent than in the purely local inhibition case. Compare Fig. 5C(iii) and 6C(iii). Interestingly, the shooting correctly predicts the velocity of the transition from the down state to the up state in the full simulation even though the steady state dynamics of the simulation are not spatially or temporally uniform. According to our numerical stability analysis, the traveling wave that joins the down state to the up state (found

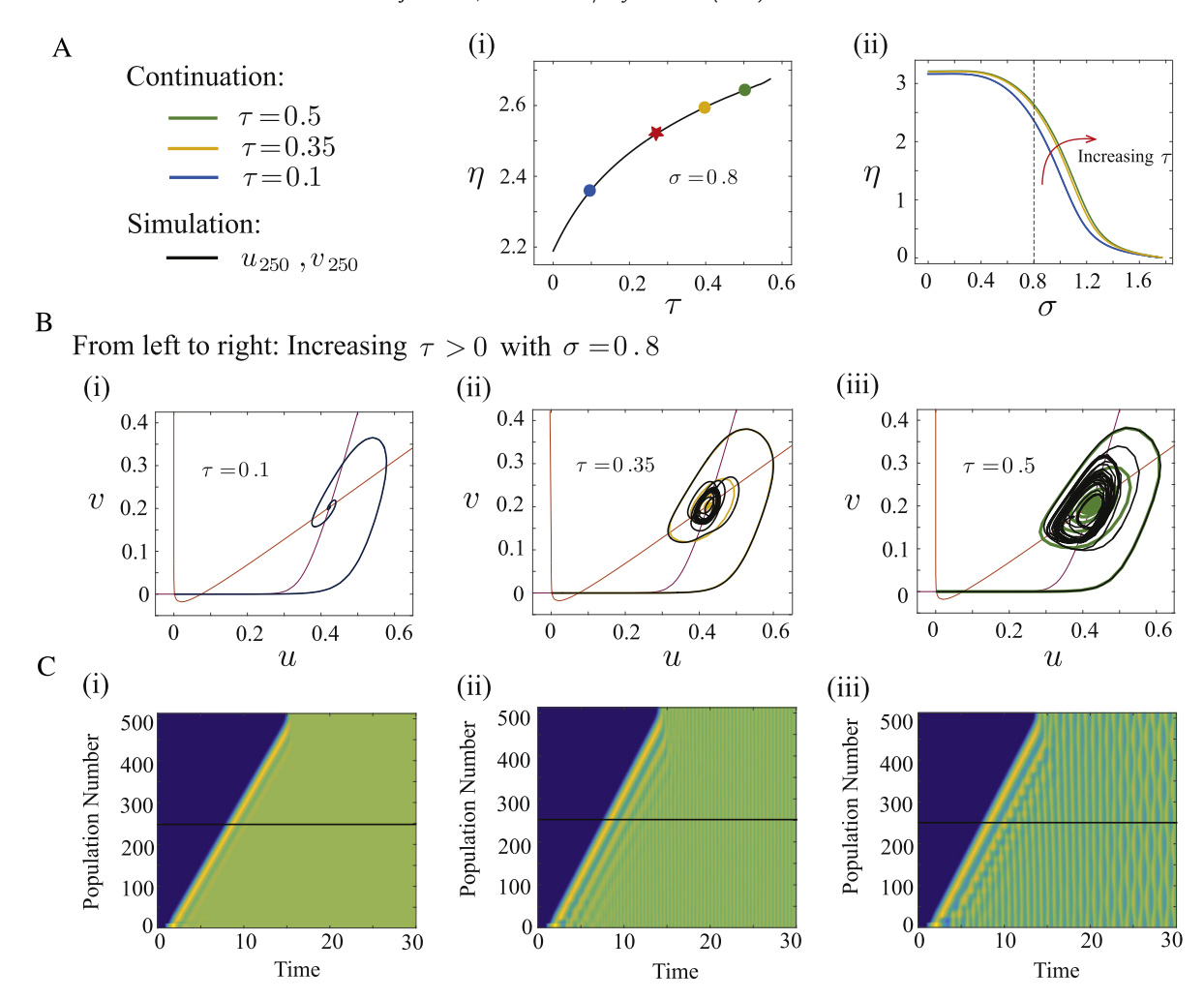


Fig. 6. Comparison of traveling front solutions of the boundary value problem with simulations of the discretized network of (N=512) excitatory and inhibitory neurons with nonlocal inhibitory connections $(\sigma_i>0)$. (A) The curve of heteroclinic orbits of the 6D system: (i) $\sigma=0.8$ in (τ,η) ; (ii) $\tau=[0.1,0.35,0.5]$ in (σ,η) parameter space. The red star at $\tau=0.2893$ is the value for which the numerical stability analysis predicts the wave goes unstable. (B) Numerical solutions and simulations in the u-v phase plane, increasing τ from left to right: (i) $\tau=0.1$, (ii) $\tau=0.35$, (iii) $\tau=0.5$. (C) Space–time plot of the excitatory population firing rates for parameters in (B).

through shooting) is unstable as a solution to the full integral equations. That is, while the front exists, it is not stable. In spite of the instability, the heteroclinic orbit provides an excellent estimate of the velocity for the down to up state activation.

2.5.3. The traveling pulse: Nonlocal inhibition

As we noted in Section 2.2, when τ is large enough, there are no attractors around the up state and, so, excursions away from the down state return to the down state. Thus, we will now look for traveling pulse solutions to Eq. (9). These can be constructed in the same manner as for the traveling front, i.e. by starting with the 4D system in Eq. (7) and then performing a shooting method to obtain solutions of the fully connected 6D system. When τ is sufficiently large, the space-clamped system is an excitable medium; that is, there is a unique globally stable down state but sufficient perturbations cause a transient excitation before decaying back to the down state. Traveling pulse solutions are often found in spatially distributed excitable media [24,28,39], so it is natural to look for such solutions in our network. Thus, in this and the next few sections, we will study the properties of traveling pulses.

Here, we increase the time constant of inhibition, $\tau > \tau_{HC} = 0.6764$, and look for a pulse solution satisfying the boundary conditions,

$$\lim_{\xi \to \pm \infty} (u, v, w, z, q, r) (\xi) = (\bar{u}, \bar{v}, \bar{u}, 0, \bar{v}, 0)_1.$$

In our analysis of the traveling pulse, we are interested in how the spatial (σ) and temporal (τ) scales affect the speed of the traveling wave as well as the stability. In Fig. 7A(i), we fix τ and continue the orbit with respect to σ . (In a subsequent section, we will fix σ and continue with respect to τ as this enables us to see the transition from fronts to pulses.) Here, we note that the speed monotonically decreases with respect to σ , which means that as the spread of inhibition increases, the wave slows down. As with fronts, the reason for this is that the inhibitory population can reach longer a range relative to the excitatory population, which slows the increase in firing rate of excitation during propagation. Moreover, the curves in (σ, η) parameter space with larger τ lie above those with smaller τ , so as with fronts, slowing the inhibition speeds up the wave. This can be explained by the fact that activation occurs through feedforward excitation of neighboring excitatory populations and is quenched by the tracking inhibition. Hence, inhibition releases excitation to spread, but a larger time scale of inhibition, means inhibitory tracking is slower in turning off excitation. In addition, we observe in Fig. 7A(ii) and (iii) that the amplitude of the pulse increases with larger τ and larger σ .

In Fig. 7B, we plot the pulse trajectory in the u-v phase plane for fixed $\tau=2$ and increasing σ to compare the trajectory from shooting (blue, yellow, green) with network simulations (black). We note that for small σ the simulations and the shooting match exactly, as in Fig. 7B(i), but there is an increasing discrepancy with

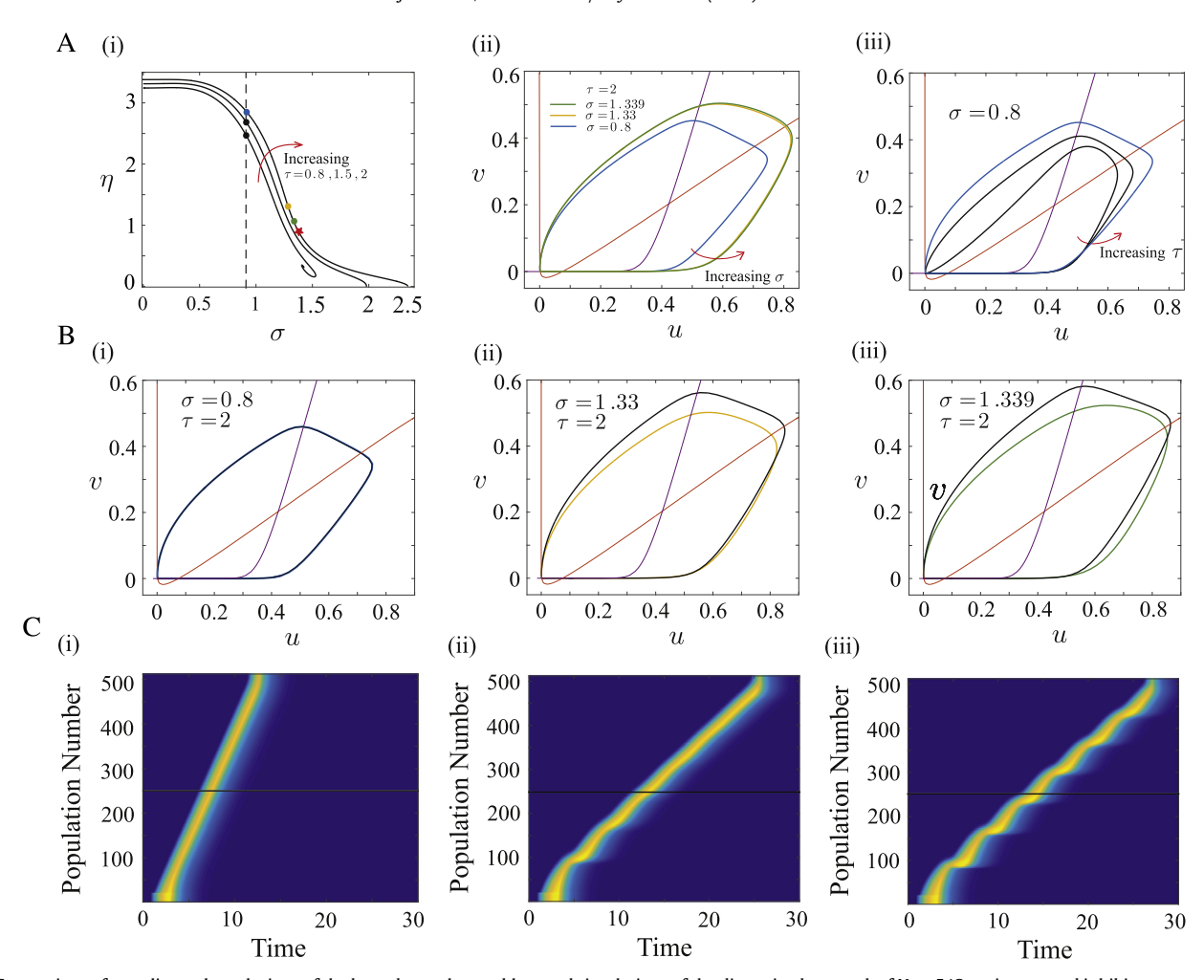


Fig. 7. Comparison of traveling pulse solutions of the boundary value problem and simulations of the discretized network of N=512 excitatory and inhibitory neurons with nonlocal inhibitory connections $(\sigma_i>0)$. (A) (i) The velocity (η) of the pulse solutions as σ varies for several different values of the inhibitory time constant: $\tau=[0.8,\ 1.5,\ 2]$. (ii) Excitatory–inhibitory (u,v) firing rates corresponding to the dots in panel (i) for $\tau=2$ and $\sigma=[0.8,\ 1.33,\ 1.339]$. The red star indicates $\sigma=1.345$, the value for which the numerical stability analysis predicts the wave goes unstable. (iii) Excitatory–inhibitory (u,v) firing rates of population for $\sigma=0.8$ and $\tau=[0.8,\ 1.5,\ 2]$ corresponding to intersections of the vertical dashed line in panel (i). (B) Numerical solutions and simulations in the u-v phase plane when $\tau=2$ and increasing σ from left to right: (i) $\sigma=0.8$, (ii) $\sigma=1.339$. (C) Space–time plot of the excitatory population firing rates for parameters in (B). (For interpretation of the references to color in this figure legend, the reader is referred to the web version of this article.)

larger values of σ , as shown in Fig. 7B(ii), (iii). This can be explained by looking at Fig. 7C where we show the full space–time plots of the excitatory firing rate for these same three values of σ . What appears to happen is that at higher values of σ (specifically, σ > 1) an instability of the pulse occurs that seems to be periodic in the traveling frame. Thus, the width of the pulse is not constant over time, and this appears to account for the discrepancy seen in Fig. 7B(ii), (iii). This type of pulse is often called a breather [40,41], or a lurching wave [42,43].

To better see the periodic orbit, we can make a coordinate change along the line $y=x+\eta t$ for the space–time arrays in Fig. 7C. These types of waves are not simply similarity solutions, as in regular traveling wave solutions, but rather, they have additional temporal dynamics. Specifically, we observe oscillations of the activated region even when transformed to the moving frame by subtracting the mean velocity of the pulse (Fig. 8B). In Fig. 8C, we see these oscillations grow with increasing σ , which indicates that the oscillation goes through a bifurcation similar to the Hopf bifurcation for a fixed point. Though the oscillatory instability to the traveling wave is apparent in the discretized simulations, continuation of the pulse solution found from shooting gives no indication. Instead, we see from Fig. 7A that the curves and orbits continue to exist, leaving from the unstable manifold and returning to the stable manifold of the down state. That is, while regular

traveling pulses continue to exist, they appear to lose stability as σ increases. We note that this instability occurs over a limited range of values of τ and σ . If τ is large, then the wave appears to just die out as σ increases, while if τ is too small, then there is no pulse. We found from our stability analysis (see Appendix E) that for $\tau = 2$, the wave goes through an instability at around $\sigma =$ 1.345 which is close to what the discretized simulations indicate in Fig. 8. Intuitively, the mechanism for lurching can be explained as follows: The larger time scale of inhibition allows for the wave to propagate quickly but the longer reach of inhibition staunches this propagation, slowing the wave down and reducing the total excitation. However, the diminished excitation and increased recurrent inhibition to the inhibitory network diminishes the inhibition, allowing the excitation to once again build up and push the wave forward. The fact that the details of the mechanism rely on a precise interplay between the temporal and spatial components of the system is consistent with our finding that the instability occurs within a small region of parameter space, specifically, at intermediate values of τ and σ .

2.6. Stimulus-dependent activation

In Fig. 6, we see that for $\sigma=0.8$ there exists a traveling front up to about $\tau=0.6$, while in Fig. 7A(i), there are pulses for at least

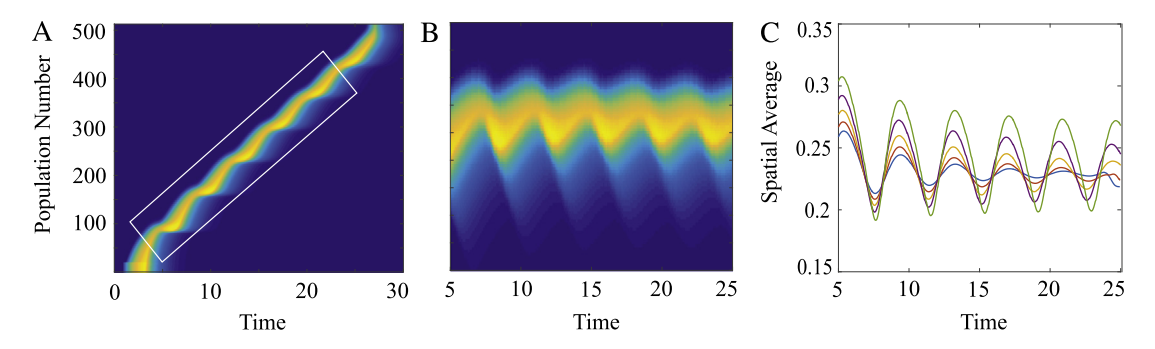


Fig. 8. Domain-straightening of the lurching wave to show the oscillatory instability as σ increases. (A) Array plot of the excitatory population firing rates when N=512, $\sigma_e=15$ and σ_i is such that $\sigma=1.339$ as in Fig. 7C(iii). (B) We estimate the speed and make a change of coordinates to transform the activated region enclosed in the rectangle shown in (A). (C) A spatial average of panel (B) gives a smooth oscillation with amplitude that grows with increasing $\sigma=[1.3, 1.31, 1.32, 1.33, 1.339]$.

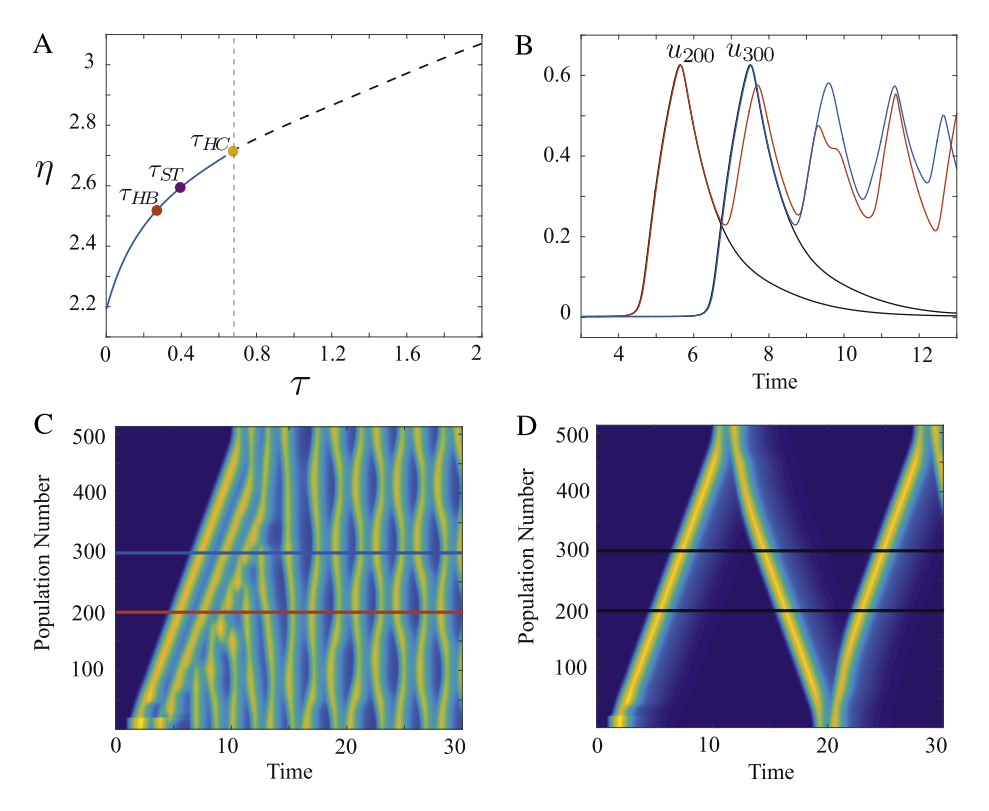


Fig. 9. Bistability near the transition from fronts to pulses. (A) Continuation of the front (solid line) and the pulse (dashed line) as the relative time scale of inhibition, τ varies for $\sigma=0.8$. The values of τ that characterize the onset of the Hopf bifurcation (HB), spatiotemporal patterns (ST), and a homoclinic (HO) are indicated. (B) Temporal evolution of a front (orange, blue) and a pulse (black) at two different spatial locations for $\tau=0.68$. (C, D) The front and the pulse in a space–time plot of the excitatory firing rate. The pulse is evoked by a stimulus lasting 1 time unit and the front, by a stimulus lasting 2.5 time units. (For interpretation of the references to color in this figure legend, the reader is referred to the web version of this article.)

 $\tau = 0.8$, and so, we try to understand how the waves make the transition from fronts to pulses as τ increases. Indeed, τ is a natural parameter to study as it does not change the equilibria of the space-clamped system but determines the stability of the up state equilibrium. Fig. 9A shows a plot for the continuation of the front (solid) and the pulse (dashed) at $\sigma = 0.8$. The front continuation terminates near the homoclinic bifurcation for the space-clamped system as does the pulse. The velocity of the traveling solutions seems to be continuous as the dynamics pass from the front to the pulse. We note that for $\tau > \tau_{HR}$, the front is unstable (cf. Fig. 6B), but the velocity matches the velocity of the front that joins the down state to the up state attractor. If we choose a value of τ near the transition point (shown by the dotted line, $\tau = 0.68$) and briefly excite a local region in the spatially discretized network, we observe that there are two kinds of attractors depending on the duration of the stimulus: Front-like for longer lasting stimuli and pulse-like for shorter lasting stimuli. These different behaviors are shown in Fig. 9C, D. The pulses appear to reflect off the boundaries, so in a semi-infinite domain, we would expect to see a traveling pulse that continued in one direction. In Fig. 9B, we show the temporal evolution of the two waves at two spatial locations. The front is depicted with the orange and blue curves and the pulse is depicted by the black curves. The temporal evolution of the front and pulse solutions look identical up until a point where the pulse drops back to the down state, while the front continues to evolve to a spatiotemporal patterned up state.

2.7. Traveling waves in the 2D model

Thus far, we have only considered the Wilson–Cowan equations on a one-dimensional spatial domain to analyze how the speed and stability of the wave depend on the temporal and spatial length scales of the system. Next, we consider a two-dimensional spatially

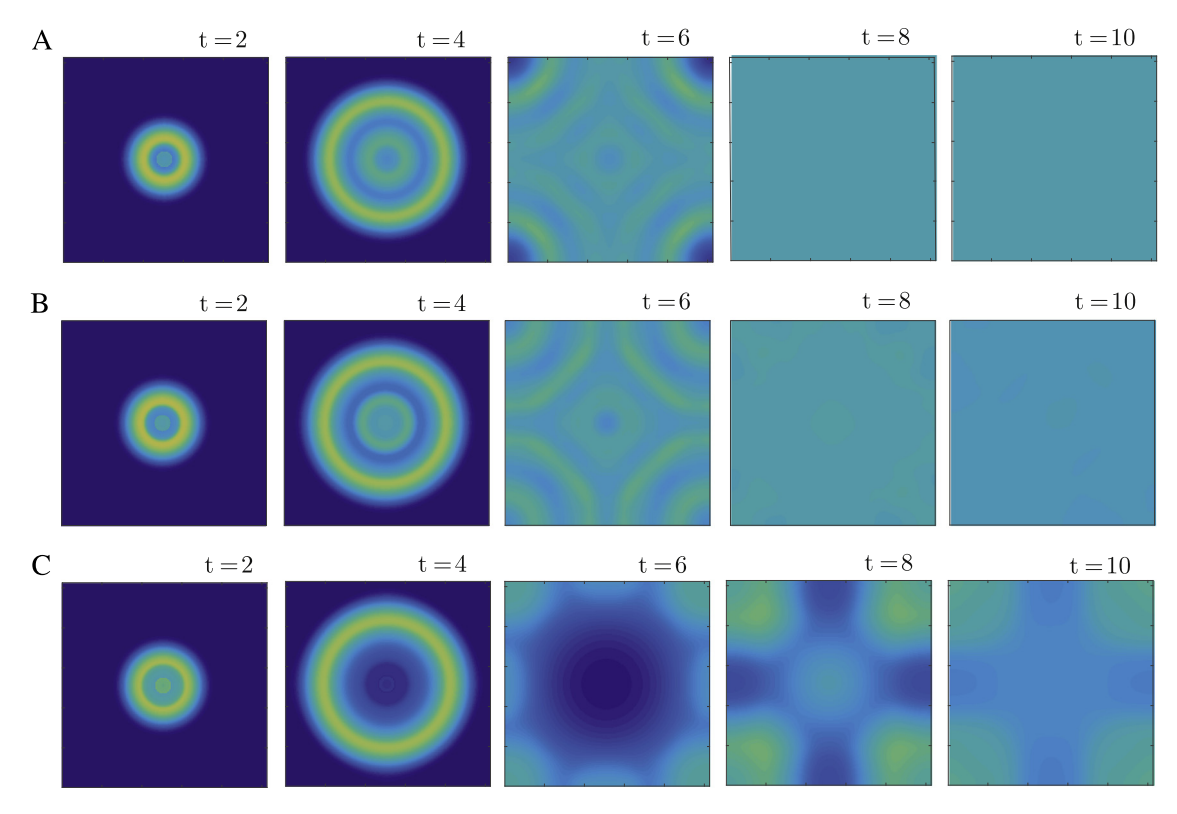


Fig. 10. Traveling fronts in the 2D spatially-distributed network (256 × 256) initiated by disc-shaped stimuli of radius 10 spatial units about the center of the media. We set $\sigma_e = 10$, $\tau_e = 1$ and show the excitatory population firing rates as a sequence of equal time frames for $\sigma_i = 9$ and three values of the inhibitory time constant: (A) $\tau_i = 0.1$; (B) $\tau_i = 0.4$; (C) $\tau_i = 0.6$.

distributed network with kernels that decay with the Euclidean distance. Here we take the kernel to be the decaying exponential,

$$K_j(\sqrt{x^2+y^2}) = \frac{1}{2\pi \sigma_j^2} \exp\left(-\frac{\sqrt{x^2+y^2}}{\sigma_j}\right) , \quad j \in \{e, i\}.$$

We can use the curves in Figs. 6 and 7 to find parameters where we might expect traveling waves in the system. To simulate the 2D spatially connected network, we create an array of 256 by 256 excitatory and inhibitory neurons with reflecting boundary conditions. We impart an initial localized stimulus and present the resulting numerical solutions in Fig. 10 as a series of five frames over equal time intervals to show the propagation. We fix $\tau_e = 1$ and $\sigma_e = 10$ and choose three different pairs of values for τ_i and σ_i to represent the three different behaviors of the up state. In Fig. 10A, the up state is a stable equilibrium, and the outwardly moving front eventually goes to a spatially uniform constant steady state. In Fig. 10B, parameters are such that the up state has a stable homogeneous oscillation and the asymptotic state of the 2D system is a spatially uniform bulk oscillation. Finally in Fig. 10C, parameters are chosen so that there is a symmetry breaking instability of the uniform oscillation in the up state and the wave transitions to that state. (See the supplemental movies for a better picture of these three types of traveling fronts.)

In Fig. 11A, we increase τ_i to 2 so that a stable pulse exists for $\sigma=0.9$. An outwardly traveling pulse appears which meets with the boundary and leaves the system back at the down state. We then increase the spatial scale of inhibition (as in Fig. 8C) to look for "lurching" waves in the 2D system. In Fig. 11B, we stimulate the upper left corner of the media (instead of the center) to show how the band of excitation propagates with varying width. From t=4 to t=6, the band of excitation contracts as inhibition catches up, and then from t=6 to t=8, it expands as feedforward excitation progresses the wave. This lurching behavior is better

seen in a space–time plot of the excitatory populations along the diagonal of the domain in panel B, which we display in Fig. 11C. In the cases where we impart a center-stimulus, we note that the outward propagation of the waves in 2D is radially symmetric in both the front and pulse simulations. Thus, it is possible to reduce the 2D system to a 1D system in order to better explore features like the velocity and magnitude of the waves. We briefly explain how to do this in Appendix D.

3. Discussion

Traveling waves in nonlocal media have been the object of a great deal of mathematical and computational study. In the context of cortical networks, experimentalists have used the waves to say something about the local circuitry of the network and have also suggested some roles for waves in sensory processing [44,45]. Waves arise when active space-clamped dynamics interact in a spatially localized manner. In almost all the studies of waves in neural fields, the space-clamped dynamics is either bistable or excitable; in the former case, the models are scalar with just a population of excitatory cells and in the latter, the space-clamped dynamics generally has a single equilibrium point. In this paper, we have considered a different type of active medium for which there are three spatially homogeneous equilibria—one of which is on the middle branch of the excitatory nullcline, which means that it is conditionally stable. This state (called the Inhibitory Stabilized Network (ISN) state [32,33] or up state) has been found to have many interesting computational features. Thus, we have focused our attention on waves that join the down state to this up state and how their existence depends on the stability of this state. For such systems, the combination of numerical shooting, continuation with AUTO, and numerical stability analysis in the comoving frame has allowed us to study how the speed and other properties of the waves depend on the inhibitory time and space scales.

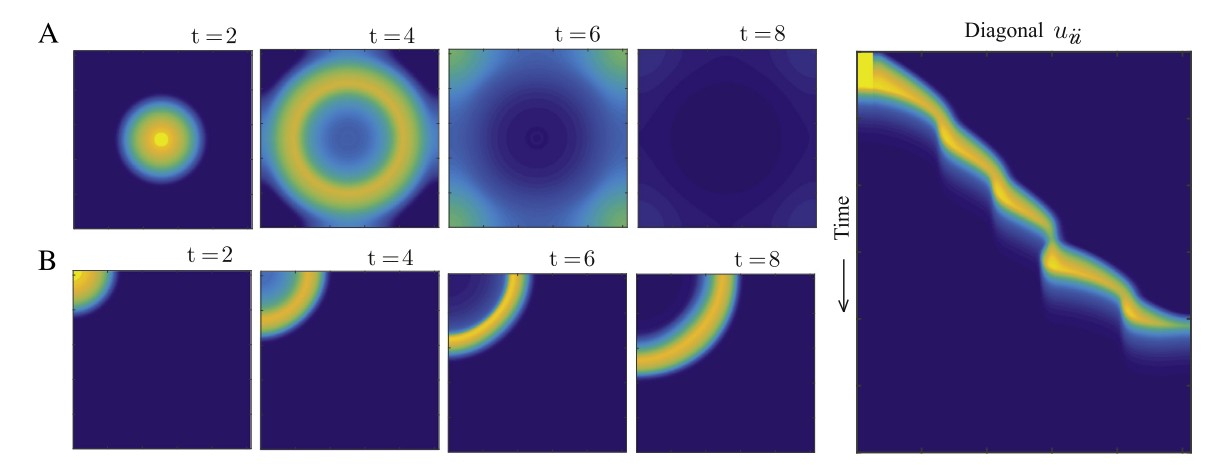


Fig. 11. Traveling pulses in the 2D spatially distributed network (256 × 256), setting $\sigma_e = 10$, $\tau_e = 1$, $\tau_i = 2$. We show the excitatory population firing rates as a sequence of equal time frames: (A) The regular traveling pulse for $\sigma_i = 9$; (B) The lurching pulse initiated in the corner for $\sigma_i = 14.5$. (C) Space–time plot along the diagonal of (B) to better illustrate the lurching behavior.

Traveling fronts in the full network correspond to heteroclinic orbits of the ODE system obtained when converting to traveling wave coordinates. These fronts take the network from the stable down state to the up state. The experiments described in [29] indicate that the transitions of cortical states from down to up are spatially organized into waves, though the transitions from up to down are not. Our results are consistent with these experiments in that we have not found fronts that transition the system from up to down state activity. It is typical for waves in bistable media to only transition in one direction (e.g. up to down or down to up, but not both). We note also that the dynamics in the up state are far richer than in the down state with oscillations and complex spatiotemporal dynamics possible. This richness could endow cortical networks with greater computational capabilities [46,47] so it makes biological sense for the transition to the up state to be organized.

While we were able to find fronts over a wide range of parameters, simulations of the discretized spatial network showed that the front did not always settle into the up state equilibrium. Indeed, as the time scale of inhibition (τ) increases, the up state goes through several bifurcations, and the front joins the down state to more complex dynamics in the up state—first leading to a spatially uniform oscillation and then to a spatiotemporal pattern. In spite of the instability, we found that the velocity determined by shooting closely matches the velocity of the full network simulation. Numerically, we found that the front loses stability at a τ -value which is greater than that of the Hopf bifurcation of the space-clamped system. Hence, there is a small interval of time scales for which the traveling front (connecting to the spatially homogeneous up state) is stabilized by nonlinearities in the comoving frame even when the spatially homogeneous up state is linearly unstable. A similar phenomenon was studied in a general reactiondiffusion system near a supercritical Hopf or Turing bifurcation of the rest state behind the front [48,49]. Their results showed that the small patterns left in the wake of the front stayed bounded and were pushed away from the front interface. Lastly, we found that further increasing the time constant of inhibition pushed the up state oscillation through a homoclinic bifurcation, and hence there was a maximum τ beyond which both simulation and numerical shooting indicated that there were no fronts of any kind.

Fronts have been well-studied in the so-called scalar model which consists of a single excitatory population. Ermentrout and McLeod [27] proved that there is a unique monotone traveling front solution to a class of scalar models with sigmoidal shaped firing rate functions and spatially decaying connections. This traveling front solution is a good approximation for the spread of

excitation when inhibition is slow. Building on these results, [28] looked at propagating fronts in the scalar model with linear adaptation, showing how the wave speed depended on the threshold for activation, spatial length scale, and synaptic decay parameters. Since then, many others [50-52] have studied traveling fronts in the scalar model with negative feedback term, either in the form of synaptic depression or spike-frequency adaptation. For instance, [50] found parameter regimes with stable counter propagating fronts by deriving an Evans function for the stability of the stationary front solution. Moreover, [51] constructed these fronts using a perturbation expansion in powers of the speed, showing a Hopf bifurcation in the case of weak input inhomogeneities and found breather-like solutions at the interface of the stationary front resulting from a modulation of the input inhomogeneity. They followed the Hopf instability for various adaptation time constants with respect to the strength of negative feedback and inhomogeneous input. [52] also studied how inhomogeneities in the media affect front propagation in the scalar model. Specifically, they modulated local excitability via changes in the slope of the firing rate function which resulted in wave speed hysteresis such that fronts moved faster when initiated on the less excitable side of the media. They further investigated this hysteresis behavior by inducing spatially dependent sinusoidal modulations of the down state and found that the difference in wave speed was linearly correlated to the gradient of the sinusoid. [52] also studied the interplay between local and nonlocal features in the scalar model. They showed a phase diagram of wave speed with respect to local and nonlocal connectivity strengths and used it to explain how the scalar model with spike-frequency adaptation might move through regions of this diagram to capture the dynamics of slowwave activity during sleep, specifically, the roughly synchronous up to down state transitions contrasted with the more sequential down to up state transitions.

The traveling pulse corresponds to a homoclinic orbit in the traveling wave frame. As with the traveling front, we compared solutions to the boundary value problem with 1D simulations of the discretized network. For pulses, we took the bifurcation parameter to be the spatial scale, $\sigma = \sigma_i/\sigma_e$, and simulations showed that the traveling pulse goes through a Hopf-like instability leading to lurching waves. Our numerical stability analysis gave a similar σ -value as to estimates found through simulation. [42] found similar oscillatory instabilities to solitary waves in an excitatory-inhibitory network of integrate-and-fire neurons in which there was an explicit delay in the coupling between the neurons. Such wave instabilities have also been studied in the scalar model with linear adaption. For instance, the authors in [40] determine the

instability of the traveling pulse for the case of the Heaviside firing rate function using an Evans function approach. Using a similar approach, [53,54] studied instabilities of a stationary pulse, referring to these types of localized oscillatory waves as 'breathers' or 'sloshers'. (The difference between the two corresponded to the destabilization of different modes, the sum or difference modes, respectively.)

Traveling pulses are a fairly common phenomena in neural tissue, both in vitro and in vivo [5,44] as well as in pathological situations [55,56] where they have been modeled without an inhibitory population of neurons. In the latter setting where inhibition is pharmacologically blocked, the scalar neural field with adaptation may be an appropriate model to study, since the negative feedback in these systems most likely arises in the local system dynamics. As previously mentioned, fronts can be obtained without adaptation [27,57], but traveling pulses will not be observed, as an inhibitory feedback mechanism is necessary to quench the activity and bring the field back to the down state equilibrium. [28,40,50,54] studied pulses in the scalar model with linear adaptation, but [57] looked at a more phenomenological neural field model for spike-frequency adaptation in which the adaptive threshold had nonlinear dynamics. In this case, instabilities to a stationary pulse lead to either breathers or traveling pulses, a richness of pulse dynamics in a homogeneous medium that is most likely attributable to the nonlinear adaptation. [58] looked at the feedback mechanism in more detail, including dynamics for both synaptic depression and nonlinear adaptation. For the parameter regime that supported pulses, they showed a phase plane and bifurcation diagram that was very similar to our space-clamped system. In their space-clamped system, they established the existence of stable limit cycles around the up state for sufficiently fast depression or adaptation. However, the intrinsic oscillation imparted different spatiotemporal effects because of the different types of traveling waves present. In their spatiallyextended system, pulses emitters arose from localized oscillations that propagated with a spatially-dependent phase shift, while in our spatially-extended model, the front traveled with one or two rebounding activations which were overtaken by a spatially homogeneous oscillation.

We also compared the wave speed curves (varying the inhibitory time constant) for the front and pulse solutions obtained through numerical shooting. We found that the transition between the two curves is continuous and occurs near the homoclinic bifurcation of the space-clamped system. To see the behavior of the network at this transition, we activated one end of the media and varied the duration of the initial stimulus. For brief stimuli, we saw pulses, while for longer stimuli we observed front-like waves that tended to a period-doubled spatiotemporal pattern. The initial activation profiles were similar between the two waves, but sufficiently long stimuli prevented the media from decaying back to rest, so waves rebounded to an activated state, [59] also found bistability between different types of traveling waves in a scalar neural field with linear adaptation. They showed a phase diagram of the front and pulse speeds as a function of adaptation strength. Different types of fronts and pulses emanated from a central bifurcation point, near which, they found bistability between a pulse and anti-pulse as well as between a pulse and inactivating front.

We began our study with localized inhibition and then made the extension to nonlocal connections in both populations, in part to illustrate our shooting method, but also to point out the differences between wave activity in the two networks: local versus nonlocal inhibition. According to our simulations and numerical analysis, the front solutions behave quite similarly in the two systems, losing stability near the Hopf bifurcation of the spatially homogeneous up state equilibrium. However, for the traveling pulses,

both simulation and numerical stability analysis indicate that the solutions behave differently: In the case of localized inhibition, the pulse is lost as the time constant of inhibition decreases but remains stable as long as it exists. In the case of nonlocal inhibition, as the time constant decreases (the spatial scale increases), the pulse loses stability at a supercritical Hopf leading to the lurching waves. This difference suggests that the interplay between the temporal and spatial scales of inhibition is key in establishing these more complicated breather-like waves.

We concluded the paper with some two-dimensional simulations that showed radially symmetric waves. We described how such waves could be analyzed in Appendix D. An alternate approach might be to use a technique used by [37] to derive a PDE model by approximating the exponential kernel with the modified Bessel function of the second kind of order zero. In this case, the Fourier transforms of the spatial kernels would become simple Hankel transforms. Based on their results, this might give an improvement over the long-wave approximation for estimating the pattern forming boundaries. A similar method was used in [54] to construct an explicit solution of a 2D stationary-pulse. These methods might be useful for further investigation of waves in the 2D spatially distributed Wilson-Cowan model. With appropriate initial conditions, we expect to also observe spiral and rotating waves similar to those found in a 2D excitatory network with nonlinear synaptic depression [60] which were initiated by breaking the rotational symmetry of pulse emitter solutions. These types of waves have been seen in cortical slices [61] and more recently in human cortex during sleep [62]. The analysis and simulation of these waves remains a topic for further study.

Acknowledgment

This work was supported by NSF DMS 1219753.

Appendix A. The linearization of the 4D and 6D systems

In this section of the appendix we show that in the 4D system, both the up and down states have a one-dimensional unstable subspace and a three-dimensional stable subspace. We then show that for the 6D system, there is a two-dimensional unstable space and a four-dimensional stable space for both fixed points. We first analyze linearizations of the 4D system at the up and down states. Putting $\sigma_e=1$, the characteristic polynomial corresponding to the 4D linearization around the up and down-states is of the form

$$p(\lambda) = \lambda^4 + A_3 \lambda^3 + A_2 \lambda^2 + A_1 \lambda + A_0$$
,

where

$$A_3 = \frac{1}{\eta} \left(1 + \frac{(1+b_{ii})}{\tau} \right) , \quad A_2 = \frac{1}{\eta^2} \left(\frac{(1+b_{ii})}{\tau} - \eta^2 \right)$$

$$\begin{split} A_1 &= -\frac{1}{\eta} \left((1-b_{ee}) + \frac{(1+b_{ii})}{\tau} \right) \ , \\ A_0 &= -\frac{1}{\eta^2 \, \tau} \, \left((1-b_{ee})(1+b_{ii}) + b_{ie} \, b_{ei} \right) \, . \end{split}$$

Note that $A_3>0$, and for $0<\tau<\tau_{HB}$, we have that $A_1\equiv\frac{Tr(0)}{\eta}<0$ and $A_0=-\frac{D(0)}{\eta^2}<0$, where Tr(0) and D(0) denote the trace and determinant of the space-clamped system. Now the sign of A_2 depends on the parameters τ and η . Nonetheless, there is one sign change between the coefficients, so applying Descartes' rule of signs, we have exactly one positive root. Looking at $p(-\lambda)$, we have three sign changes (regardless of the sign of A_2), so Descartes' rule gives three or one negative roots.

Around the *down-state*, we found numerically that for the given parameters $\bar{u}=2.1443\times 10^{-3}$ and $\bar{v}=2.2944\times 10^{-9}$. Hence the

terms $b_{ee} = a_{ei}\beta\bar{v}\,(1-\bar{v})$ and $b_{ei} = a_{ei}\beta\bar{v}\,(1-\bar{v})$ are of order $O(10^{-1})$, while the terms $b_{ie} = a_{ie}\beta\bar{v}\,(1-\bar{v})$ and $b_{ii} = a_{ii}\beta\bar{v}\,(1-\bar{v})$ are of order $O(10^{-7})$. Setting $b_{ie} = b_{ii} = 0$, a good approximation for the characteristic polynomial is

$$\begin{split} p(\lambda) &= \lambda^4 + \frac{1}{\eta} \left(1 + \frac{1}{\tau} \right) \lambda^3 + \frac{1}{\eta^2} \left(\frac{1}{\tau} - \eta^2 \right) \lambda^2 \\ &- \frac{1}{\eta} \left((1 - b_{ee}) + \frac{1}{\tau} \right) \lambda - \frac{(1 - b_{ee})}{\eta^2 \tau} \,, \end{split}$$

which has a zero at $\lambda = -\frac{1}{n\tau} < 0$. We further factor to obtain,

$$p(\lambda) = \left(\lambda + \frac{1}{\eta \tau}\right) q(\lambda),$$

where $q(\lambda)=\lambda^3+\frac{1}{\eta}\,\lambda^2-\lambda-\frac{(1-b_{ee})}{\eta}$. Since $q(\lambda)$ has exactly one positive root, then the remaining two roots are either negative or form a complex conjugate pair. Note that $q\left(-\frac{1}{\eta}\right)=\frac{b_{ee}}{\eta}>0$ and $q(0)=-\frac{(1-b_{ee})}{\eta}<0$, so by the Intermediate Value Theorem, there is at least one real root on the interval $(-\frac{1}{\eta},0)$, which then gives two negative roots of $q(\lambda)$. Hence the down-state has a three dimensional stable manifold and one dimensional unstable manifold.

If we homotopy from the down to up-state so that the coefficients b_{ii} move (continuously) away from zero, then we can follow (continuously) the roots of the resulting family of polynomials. Now we want to show that the three dimensional stable manifold is preserved under this homotopy. Around the up-state, Descartes' rule of signs still gives a one positive root and (at least) one negative root of $p(\lambda)$ when $0 < \tau < \tau_{HB}$, so we consider how the two additional negative roots starting in the down-state can pass through the imaginary axis. One case is through a zero eigenvalue, which is not possible, since $A_0 < 0$. The other is through a complex conjugate pair passing through the imaginary axis, in which case there must be a point when the real part is zero and the pair is of the form $\lambda = \pm \omega i$ with $\omega \in \mathbb{R}$. Looking at $p(\omega i)$, the imaginary terms must cancel, so we have the necessary condition: $-A_3 \omega^2 + A_1 = 0$. Since $A_3 > 0$ and $A_1 < 0$, this is impossible. Hence, the up-state has a three dimensional stable manifold and one dimensional unstable manifold.

Now we study the 6D linearization and use similar arguments as in the 4D linearization to show that for certain values of τ and $\sigma = \sigma_e/\sigma_i$ the up and down-states have four dimensional stable manifolds and two dimensional unstable manifold. We write the characteristic polynomial:

$$f(\lambda) = \lambda^6 + C_5 \lambda^5 + C_4 \lambda^4 + C_3 \lambda^3 + C_2 \lambda^2 + C_1 \lambda + C_0$$

where

$$\begin{split} C_5 &= \frac{1}{\eta \, \tau} \, (1 + \tau) \quad , \qquad C_4 = -1 - \frac{1}{\sigma^2} + \frac{1}{\eta^2 \, \tau} \quad , \\ C_3 &= -\frac{1}{\eta} \left(1 - b_{ee} + \frac{1}{\tau} + \frac{1}{\sigma^2} \left(1 + \frac{1 + b_{ii}}{\tau} \right) \right) \end{split}$$

$$\begin{split} C_2 &= -\frac{1}{\eta^2 \, \tau} \left(1 - b_{ee} + \frac{1}{\sigma^2} \left(\eta^2 \, \tau + 1 + b_{ii} \right) \right) &, \\ C_1 &= \frac{1}{\eta \, \sigma^2} \left(1 - b_{ee} + \frac{1 + b_{ii}}{\tau} \right) &, \\ C_0 &= \frac{1}{n^2 \, \sigma^2 \, \tau} \, \left((1 - b_{ee})(1 + b_{ii}) + b_{ie} \, b_{ei} . \right) \end{split}$$

Note that $C_5>0$. Also, for $0<\tau<\tau_{HB}$, $C_1=-\frac{Tr(0)}{\eta\,\sigma^2}>0$ and $C_0=\frac{D(0)}{\eta^2\,\tau^2}>0$. If in addition $0<\sigma<1$, then $C_3<0$. Independent of the sign of C_4 , we have two sign changes when ordering the

coefficients. Hence, we have either two or zero positive roots. Considering $f(-\lambda)$, we see that there are four sign changes, which gives four, two, or zero negative roots. Setting $b_{ie}=b_{ii}=0$ as before, we obtain an approximation for the characteristic polynomial around the down-state:

$$g(\lambda) = \left(\lambda^2 - \frac{1}{\sigma^2}\right) p(\lambda).$$

Hence, we gain two real roots: One positive and one negative. Then the down-state has a four dimensional stable manifold and a two dimensional unstable manifold. Using a similar homotopy argument as in the 4D linearization, we can show this stability structure is preserved as we move b_{ie} and b_{ii} away from zero. A positive eigenvalue cannot be gained from a negative eigenvalue, as $C_0 = \frac{D(0)}{\eta^2 \tau^2} > 0$. Now suppose a complex conjugate pair (with negative real part) passes through the imaginary axis, i.e. $\lambda = \pm \omega i$ with $\omega > 0$ at some point. Looking at $g(\omega i)$, we must have $0 = C_5 \omega^4 - C_3 \omega^2 + C_1 = C_5 (\omega^2)^2 - C_3 (\omega^2) + C_1$, but since $C_5 > 0$, $C_3 < 0$ and $C_1 > 0$, there are no positive roots. Hence there is no solution such that ω is real, and so, purely imaginary eigenvalues are not possible. Thus, both the up and down-states have four dimensional stable manifolds and two dimensional unstable manifolds.

Appendix B. A homotopy from local to nonlocal inhibition

Briefly, we describe our continuation methods to obtain traveling wave solutions of the 6D system in Eq. (9). Let $v_{\lambda} := (1 - \lambda) v + \lambda q$ with homotopy parameter $\lambda \in [0, 1]$. We write the system:

$$\eta u' = (-u + F(a_{ee} w - a_{ei} v_{\lambda} - \theta_{e}))
(\eta \tau) v' = (-v + F(a_{ie} w - a_{ii} v_{\lambda} - \theta_{i}))
w' = z
z' = (w - u)
q' = r
r' = (a - v)/\sigma.$$
(11)

When $\lambda=0$, we have $v_{(\lambda=0)}=v$ so that the first four equations are decoupled from the last two, and this becomes a more manageable shooting problem (varying $\eta>0$) for Eq. (6). The last two equations 'see' the dynamics of v and have one dimensional stable and unstable manifolds. Once $\eta>0$ is fixed, the dynamics for v are approximated and we can vary $\sigma>0$ to solve for the heteroclinic or homoclinic orbit in the (q,r) system. With an initial approximation of the orbit, we make the 'period' larger. In practice, before coupling the (u,v,w,z) system by continuing λ from 0 to 1, the parameter $\sigma>0$ may need to be decreased. In Fig. 12, we illustrate the homotopy of heteroclinic solutions for $\sigma=0.9$, $\tau=0.1$ by plotting the trajectory in the u-v and q-r planes and increasing the homotopy parameter λ from 0 to 1.

Appendix C. Analysis of standing waves

In Fig. 7, we see that for $\tau > 0$ large enough the speed of the traveling pulse goes to zero as $\sigma > 0$ increases. Analytically, these waves correspond to $\eta = 0$ so that the time-invariant solutions u(x), v(x) can be put in terms of (w, z, q, r)(x):

$$u(x) = F(a_{ee}w(x) - a_{ei}q(x) - \theta_e)$$

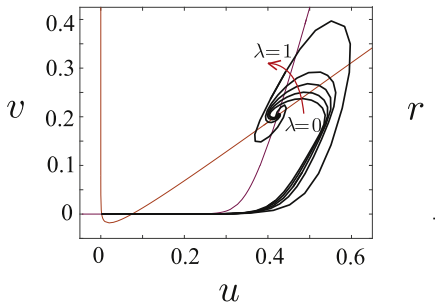
$$v(x) = F(a_{ie}w(x) - a_{ii}q(x) - \theta_i)$$
(12)

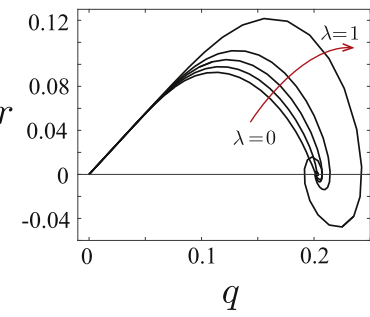
where the remaining variables (w, z, q, r)(x) satisfy the boundary value problem:

$$w' = z$$

$$z' = (w - u)$$

$$q' = r$$
(13)





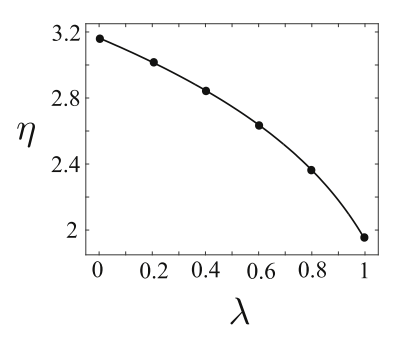


Fig. 12. A homotopy of heteroclinic solutions: Increasing $\lambda = [0, 0.2, 0.4, 0.6, 0.8, 1]$ to go from the localized solutions to nonlocal solutions. Compare the orbits $\lambda = 0$ to Fig. 5B(i) and $\lambda = 1$ to Fig. 6B(i).

$$\lambda^{2} = \frac{(1 - b_{ee} - (1 + b_{ii})/\sigma) \pm \sqrt{(1 - b_{ee} - (1 + b_{ii})/\sigma)^{2} - 4((1 - b_{ee})(1 + b_{ii})/\sigma + b_{ie} b_{ei}/\sigma)}}{2}$$

Box I.

$$\begin{split} r' &= (q-v)/\sigma \\ \lim_{x\to\pm\infty} \left(w,\,z,\,q,\,r\right)(x) &= \left(\bar{u},\,0,\,\bar{v},0\right)_1 \,. \end{split}$$

This is a 4D nonlinear differential equation with $'=\frac{d}{dx}$. Since these are time-invariant solutions, the temporal scale τ is no longer a parameter of the system. The linearization around the down-state and corresponding eigenvectors are

$$\begin{pmatrix} 0 & 1 & 0 & 0 \\ 1 - b_{ee} & 0 & b_{ei} & 0 \\ 0 & 0 & 0 & 1 \\ -b_{ie}/\sigma & 0 & (1 + b_{ii})/\sigma & 0 \end{pmatrix} , \begin{pmatrix} b_{ei} \\ \lambda & b_{ei} \\ (\lambda^2 + b_{ee} - 1) \\ \lambda & (\lambda^2 + b_{ee} - 1) \end{pmatrix},$$

where the eigenvalues satisfy

$$\lambda^{4} - (1 - b_{ee} - (1 + b_{ii}) / \sigma) \lambda^{2} + (1 - b_{ee}) (1 + b_{ii}) / \sigma + b_{ie} b_{ei} / \sigma = 0.$$

Both solutions (given in Box I) are real and positive. Hence the eigenvalues take the form $\pm \sqrt{c_1}$ and $\pm \sqrt{c_2}$ where c_1 , $c_2 > 0$, and the down-state E_1 has two positive and two negative eigenvalues. Unfortunately, numerically obtaining a homoclinic orbit connecting the two dimensional unstable manifold to the two dimensional stable manifold of the down-state is a difficult task, since initial perturbations of the trajectory should be linear combinations of the eigenvectors corresponding to the unstable directions, which depend on the parameter $\sigma > 0$.

Appendix D. Analysis of 2D traveling waves: A reduction to 1D

A possible method for analyzing the traveling waves found in our 2D spatial model is to exploit the radial symmetry of traveling waves initiated by a circular-shaped stimulus located at the center of the media. The strategy is to convert the system to polar coordinates, wherein the convolutions become special functions and the spatial dimension is reduced to one. Since these waves are independent of the polar angle, we can integrate out the angle to define the kernel

$$J(r,r') = \frac{2\pi}{\sigma^2} \, \exp\left(-\frac{r^2}{2\sigma^2}\right) \, I_0\left(\frac{r\,r'}{\sigma^2}\right) \left\lceil r' \exp\left(-\frac{r'^2}{2\,\sigma^2}\right) \right\rceil \,,$$

where $I_0(x) = \int_0^{\pi} \exp(x \cos(\phi)) d\phi$ denotes the modified Bessel Function of the first kind. Then the 2D spatial convolution terms

become radially-dependent 1D integrals:

$$(K \star u)(r,t) = \int_0^\infty J(r,r') u(r',t) dr'.$$

Then one can analyze the partial integro-differential equation in radial coordinates given by

$$\frac{\partial u}{\partial t}(r,t) = -u(r,t) + F\left(a_{ee} \int_0^\infty J_e(r,r') u(r',t) dr'\right)
- a_{ei} \int_0^\infty J_i(r,r') v(r',t) dr' - \theta_e
\tau \frac{\partial v}{\partial t}(r,t) = -v(r,t) + F\left(a_{ie} \int_0^\infty J_e(r,r') u(r',t) dr'\right)
- a_{ii} \int_0^\infty J_i(r,r') v(r',t) dr' - \theta_i .$$
(14)

Appendix E. Numerical stability analysis

It is nontrivial to determine the stability of the traveling waves for smooth nonlinearities as it is not possible to reduce the question to a simple Evans function (which is the case when the nonlinearities are piecewise constant). Instead, we spatially discretize the network (as we have done in the simulations), and instead of solving in terms of x, t, we solve in terms of $\xi = x - \eta t$ and t. Hence we have to solve the system

$$u_{t} = -u + \eta u_{\xi} + f(a_{ee}K_{e}(\xi) \star u(\xi, t) - a_{ei}K_{i}(\xi) \star v(\xi, t) - \theta_{e})$$

$$\tau v_{t} = -v + \eta \tau v_{\xi} + f(a_{ie}K_{e}(\xi) \star u(\xi, t) - a_{ii}K_{i}(\xi) \star v(\xi, t) - \theta_{i}),$$

where η must be chosen so that the wave is a *fixed* point of this evolution problem. Note that η will be the velocity of the traveling wave. We discretized these equations into N=256 bins for each component, u and v, with $\Delta x=0.1$. The convolutions were done over a periodic domain for the pulse, since the endpoints are equal and with reflecting boundary conditions for the front. We used a centered difference for the derivative in ξ . We fix the wave in ξ by demanding that we also have $u(\xi_0)=u_0$ where ξ_0 is chosen to be some point in the interior of our discretized domain. We then seek a fixed point of the resulting set of ODEs. Having found a fixed point (that is, choosing η correctly so that the wave does not move), we then linearize the ODEs around the fixed point, compute the eigenvalues of the resulting large (512 \times 512) matrix and search for the eigenvalues that have small real parts (other than the

zero eigenvalue that comes from the translation invariance of the wave). We adjust parameters by hand until we can find the values at which the real part of an eigenvalue crosses 0. We do this both for the pulse and the front. We note that this approach for finding the wave speed and the stability can be used for any convolution kernel and does not require the special case of an exponential.

Appendix F. Supplementary data

Supplementary material related to this article can be found online at https://doi.org/10.1016/j.physd.2017.12.011.

References

- R.D. Traub, J.G. Jefferys, Richard Miles, Analysis of the propagation of disinhibition-induced after-discharges along the guinea-pig hippocampal slice in vitro, J. Physiol. 472 (1993) 267.
- [2] R.D. Chervin, P.A. Pierce, B.W. Connors, Periodicity and directionality in the propagation of epileptiform discharges across neocortex, J. Neurophysiol. 60 (5) (1988) 1695–1713.
- [3] J. Julius Zhu, Barry W. Connors, Intrinsic firing patterns and whisker-evoked synaptic responses of neurons in the rat barrel cortex, J. Neurophysiol. 81 (3) (1999) 1171–1183.
- [4] W. Bryan Wilent, Diego Contreras, Synaptic responses to whisker deflections in rat barrel cortex as a function of cortical layer and stimulus intensity, J. Neurosci. 24 (16) (2004) 3985–3998.
- [5] Lyle Muller, Alexandre Reynaud, Frédéric Chavane, Alai Destexhe, The stimulus-evoked population response in visual cortex of awake monkey is a propagating wave, Nature Commun. 5 (2014).
- [6] David Golomb, Yael Amitai, Propagating neuronal discharges in neocortical slices: computational and experimental study, J. Neurophysiol. 78 (3) (1997) 1199–1211.
- [7] Adam Keane, Pulin Gong, Propagating waves can explain irregular neural dynamics, J. Neurosci. 35 (4) (2015) 1591–1605.
- [8] John P. Donoghue, Jerome N. Sanes, Nicholas G. Hatsopoulos, Gyöngyi Gaál, Neural discharge and local field potential oscillations in primate motor cortex during voluntary movements, J. Neurophysiol. 79 (1) (1998) 159–173.
- [9] Doug Rubino, Kay A. Robbins, Nicholas G. Hatsopoulos, Propagating waves mediate information transfer in the motor cortex, Nature Neurosci. 9 (12) (2006) 1549–1557.
- [10] Kazutaka Takahashi, Maryam Saleh, Richard D. Penn, Nicholas Hatsopoulos, Propagating waves in human motor cortex, Front. Hum. Neurosci. 5 (2011) 40.
- [11] Stewart Heitmann, Pulin Gong, Michael Breakspear, A computational role for bistability and traveling waves in motor cortex, Front. Comput. Neurosci. 6 (2012) 67.
- [12] Stewart Heitmann, Tjeerd Boonstra, Michael Breakspear, A dendritic mechanism for decoding traveling waves: principles and applications to motor cortex, PLoS Comput. Biol. 9 (10) (2013) e1003260.
- [13] Theodoros P. Zanos, Patrick J. Mineault, Konstantinos T. Nasiotis, Daniel Guitton, Christopher C. Pack, A sensorimotor role for traveling waves in primate visual cortex, Neuron 85 (3) (2015) 615–627.
- [14] Kyle E. Mathewson, Christopher Prudhomme, Monica Fabiani, Diane M. Beck, Alejandro Lleras, Gabriele Gratton, Making waves in the stream of consciousness: entraining oscillations in eeg alpha and fluctuations in visual awareness with rhythmic visual stimulation, J. Cogn. Neurosci. 24 (12) (2012) 2321–2333.
- [15] Georgios Michalareas, Julien Vezoli, Stan Van Pelt, Jan-Mathijs Schoffelen, Henry Kennedy, Pascal Fries, Alpha-beta and gamma rhythms subserve feedback and feedforward influences among human visual cortical areas, Neuron 89 (2) (2016) 384–397.
- [16] David J. Pinto, Saundra L. Patrick, Wendy C. Huang, Barry W. Connors, Initiation, propagation, and termination of epileptiform activity in rodent neocortex in vitro involve distinct mechanisms, J. Neurosci. 25 (36) (2005) 8131–8140.
- [17] Andrew J. Trevelyan, David Sussillo, Brendon O. Watson, Rafael Yuste, Modular propagation of epileptiform activity: evidence for an inhibitory veto in neocortex, J. Neurosci. 26 (48) (2006) 12447–12455.
- [18] Y. Chagnac-Amitai, B.W. Connors, Horizontal spread of synchronized activity in neocortex and its control by gaba-mediated inhibition, J. Neurophysiol. 61 (4) (1989) 747–758.
- [19] Alan L. Hodgkin, Andrew F. Huxley, A quantitative description of membrane current and its application to conduction and excitation in nerve, J. Physiol. 117 (4) (1952) 500.
- [20] Richard FitzHugh, Impulses and physiological states in theoretical models of nerve membrane, Biophys. J. 1 (6) (1961) 445–466.
- [21] Jinichi Nagumo, Suguru Arimoto, Shuji Yoshizawa, An active pulse transmission line simulating nerve axon, Proc. IRE 50 (10) (1962) 2061–2070.

- [22] Robert B. Levy, Alex D. Reyes, Spatial profile of excitatory and inhibitory synaptic connectivity in mouse primary auditory cortex, J. Neurosci. 32 (16) (2012) 5609–5619.
- [23] Stephen Coombes, Peter beim Graben, Roland Potthast, James Wright, Neural Fields, Springer, 2014.
- [24] Shun-ichi Amari, Dynamics of pattern formation in lateral-inhibition type neural fields, Biol. Cybern. 27 (2) (1977) 77–87.
- [25] Bard Ermentrout, Neural networks as spatio-temporal pattern-forming systems, Rep. Prog. Phys. 61 (4) (1998) 353.
- [26] Stephen Coombes, Waves, bumps, and patterns in neural field theories, Biol. Cybern. 93 (2) (2005) 91–108.
- [27] G. Bard Ermentrout, J. Bryce McLeod, Existence and uniqueness of travelling waves for a neural network, Proc. R. Soc. Edinburgh A 123 (3) (1993) 461–478.
- [28] David J. Pinto, G. Bard Ermentrout, Spatially structured activity in synaptically coupled neuronal networks: I. Traveling fronts and pulses, SIAM J. Appl. Math. 62 (1) (2001) 206–225.
- [29] Artur Luczak, Peter Barthó, Stephan L. Marguet, György Buzsáki, Kenneth D. Harris, Sequential structure of neocortical spontaneous activity in vivo, Proc. Natl. Acad. Sci. 104 (1) (2007) 347–352.
- [30] Paul C. Fife, J. Bryce McLeod, The approach of solutions of nonlinear diffusion equations to travelling front solutions, Arch. Ration. Mech. Anal. 65 (4) (1977) 335–361.
- [31] Yousheng Shu, Andrea Hasenstaub, David A. McCormick, Turning on and off recurrent balanced cortical activity, Nature 423 (6937) (2003) 288–293.
- [32] Hirofumi Ozeki, Ian M. Finn, Evan S. Schaffer, Kenneth D. Miller, David Ferster, Inhibitory stabilization of the cortical network underlies visual surround suppression, Neuron 62 (4) (2009) 578–592.
- [33] Misha V. Tsodyks, William E. Skaggs, Terrence J. Sejnowski, Bruce L. McNaughton, Paradoxical effects of external modulation of inhibitory interneurons, J. Neurosci. 17 (11) (1997) 4382–4388.
- [34] G. Bard Ermentrout, David H. Terman, Mathematical Foundations of Neuroscience, Vol. 35, Springer Science & Business Media, 2010.
- [35] Rehman Ali, Jeremy Harris, Bard Ermentrout, Pattern formation in oscillatory media without lateral inhibition, Phys. Rev. E 94 (1) (2016) 012412.
- [36] Carlo R. Laing, William C. Troy, Pde methods for nonlocal models, SIAM J. Appl. Dyn. Syst. 2 (3) (2003) 487–516.
- [37] Stephen Coombes, N.A. Venkov, L. Shiau, Ingo Bojak, David T.J. Liley, Carlo R. Laing, Modeling electrocortical activity through improved local approximations of integral neural field equations, Phys. Rev. E 76 (5) (2007) 051901.
- [38] Bard Ermentrout, Simulating, Analyzing, and Animating Dynamical Systems: A Guide to XPPAUT for Researchers and Students, SIAM, 2002.
- [39] Paul C. Bressloff, Waves in neural media, in: Lecture Notes on Mathematical Modelling in the Life Sciences, Springer, New York, 2014.
- [40] Stefanos E. Folias, Paul C. Bressloff, Stimulus-locked traveling waves and breathers in an excitatory neural network, SIAM J. Appl. Math. 65 (6) (2005) 2067–2092.
- [41] Stefanos E. Folias, Traveling waves and breathers in an excitatory-inhibitory neural field, Phys. Rev. E 95 (3) (2017) 032210.
- [42] David Golomb, G. Bard Ermentrout, Continuous and lurching traveling pulses in neuronal networks with delay and spatially decaying connectivity, Proc. Natl. Acad. Sci. 96 (23) (1999) 13480–13485
- [43] S. Coombes, P.C. Bressloff, Saltatory waves in the spike-diffuse-spike model of active dendritic spines, Phys. Rev. Lett. 91 (2) (2003) 028102.
- [44] Jian-Young Wu, Xiaoying Huang, Chuan Zhang, Propagating waves of activity in the neocortex: what they are, what they do, The Neuroscientist 14(5)(2008) 487–502
- [45] D. Kleinfeld, K.R. Delaney, M.S. Fee, J.A. Flores, D.W. Tank, A. Gelperin, Dynamics of propagating waves in the olfactory network of a terrestrial mollusk: an electrical and optical study, J. Neurophysiol. 72 (3) (1994) 1402–1419.
- [46] Carl van Vreeswijk, Haim Sompolinsky, Chaotic balanced state in a model of cortical circuits, Neural Comput. 10 (6) (1998) 1321–1371.
- [47] Misha V. Tsodyks, Terrance Sejnowski, Rapid state switching in balanced cortical network models, Network: Comput. Neural Syst. 6 (2) (1995) 111–124.
- [48] Margaret Beck, Anna Ghazaryan, Björn Sandstede, Nonlinear convective stability of travelling fronts near turing and hopf instabilities, J. Differential Equations 246 (11) (2009) 4371–4390.
- [49] Anna Ghazaryan, Björn Sandstede, Nonlinear convective instability of turingunstable fronts near onset: a case study, SIAM J. Appl. Dyn. Syst. 6 (2) (2005) 319–347
- [50] Stephen Coombes, Markus R. Owen, Evans functions for integral neural field equations with heaviside firing rate function, SIAM J. Appl. Dyn. Syst. 3 (4) (2004) 574–600.
- [51] Paul C. Bressloff, Stefanos E. Folias, Front bifurcations in an excitatory neural network, SIAM J. Appl. Math. 65 (1) (2004) 131–151.
- [52] Cristiano Capone, Maurizio Mattia, Speed hysteresis and noise shaping of traveling fronts in neural fields: role of local circuitry and nonlocal connectivity, Sci. Rep. 7 (2017).
- [53] Stefanos E. Folias, Nonlinear analysis of breathing pulses in a synaptically coupled neural network, SIAM J. Appl. Dyn. Syst. 10 (2) (2011) 744–787.

- [54] Stefanos E. Folias, Paul C. Bressloff, Breathing pulses in an excitatory neural network, SIAM J. Appl. Dyn. Syst. 3 (3) (2004) 378–407.
- [55] David J. Pinto, Saundra L. Patrick, Wendy C. Huang, Barry W. Connors, Initiation, propagation, and termination of epileptiform activity in rodent neocortex in vitro involve distinct mechanisms, J. Neurosci. 25 (36) (2005) 8131–8140.
- [56] Mark A. Kramer, Sydney S. Cash, Epilepsy as a disorder of cortical network organization, The Neuroscientist 18 (4) (2012) 360–372.
- [57] Stephen Coombes, Markus R. Owen, Bumps, breathers, and waves in a neural network with spike frequency adaptation, Phys. Rev. Lett. 94 (14) (2005) 148102
- [58] Zachary P. Kilpatrick, Paul C. Bressloff, Effects of synaptic depression and adaptation on spatiotemporal dynamics of an excitatory neuronal network, Physica D 239 (9) (2015) 547–560.
- [59] Hil G.E. Meijer, Stephen Coombes, Travelling waves in models of neural tissue: from localised structures to periodic waves, EPJ Nonlinear Biomed. Phys. 2 (1) (2014) 3
- [60] Zachary P. Kilpatrick, Paul C. Bressloff, Spatially structured oscillations in a two-dimensional excitatory neuronal network with synaptic depression, J. Comput. Neurosci. 28 (2) (2010) 193–209.
- [61] Xiaoying Huang, William C. Troy, Qian Yang, Hongtao Ma, Carlo R. Laing, Steven J. Schiff, Jian-Young Wu, Spiral waves in disinhibited mammalian neocortex, J. Neurosci. 24 (44) (2004) 9897–9902.
- [62] Lyle Muller, Giovanni Piantoni, Dominik Koller, Sydney S. Cash, Eric Halgren, Terrence J. Sejnowski, Rotating waves during human sleep spindles organize global patterns of activity that repeat precisely through the night, eLife 5 (2016) e17267.